2017

A study of particle beam spin dynamics for high precision experiments

Andrew J. Fiedler

ABSTRACT

A STUDY OF PARTICLE BEAM SPIN DYNAMICS FOR HIGH PRECISION EXPERIMENTS

Andrew J. Fiedler, MS
Department of Physics
Northern Illinois University, 2017
Michael Syphers, Director

In the search for physics beyond the Standard Model, high precision experiments to measure fundamental properties of particles are an important frontier. One group of such measurements involves magnetic dipole moment (MDM) values as well as searching for an electric dipole moment (EDM), both of which could provide insights about how particles interact with their environment at the quantum level and if there are undiscovered new particles. For these types of high precision experiments, minimizing statistical uncertainties in the measurements plays a critical role.

This work leverages computer simulations to quantify the effects of statistical uncertainty for experiments investigating spin dynamics. In it, analysis of beam properties and lattice design effects on the polarization of the beam is performed. As a case study, the beam lines that will provide polarized muon beams to the Fermilab Muon g-2 experiment are analyzed to determine the effects of correlations between the phase space variables and the overall polarization of the muon beam.

NORTHERN ILLINOIS UNIVERSITY
DE KALB, ILLINOIS

MAY 2017

A STUDY OF PARTICLE BEAM SPIN DYNAMICS FOR HIGH PRECISION EXPERIMENTS

BY

ANDREW J. FIEDLER

A THESIS SUBMITTED TO THE GRADUATE SCHOOL

IN PARTIAL FULFILLMENT OF THE REQUIREMENTS

FOR THE DEGREE

MASTER OF SCIENCE

DEPARTMENT OF PHYSICS

Thesis Director:
Michael Syphers

ACKNOWLEDGEMENTS

The author would like to acknowledge the great assistance and guidance of Michael Syphers and Diktys Stratakis, who lent their expertise and patience as I was learning the basics of accelerators and simulation software. I would also thank Aakaash Narayanan and Sebastain Szustkowski who proved excellent reviewers and sounding boards for troubleshooting problems with keen questions and insights.

I also thank Maxim Korostelev, who had performed a similar analysis for the g-2 collaboration using different software, for his generosity in sharing the results for the comparison plots made in Chapter 4. The particle distributions were created through efforts from Maxim as well as Valodja Tishchenko.

The picture of the delivery system with the beamlines labeled (in Chapter 3) was created by Brian Drendel, and I greatly appreciate his permission to use it.

This work was supported by the National Science Foundation Grant 1623691. A portion of the work was performed at Fermi National Accelerator Laboratory which is operated by the Fermi Research Alliance, LLC under Contract No. DE-AC02-07CH11359 with the United States Department of Energy.

DEDICATION

For the generosity and support of allowing a 29-year-old to move in while he steered his life in a new direction, I dedicate this work to my mother and father.

TABLE OF CONTENTS

LIST OF TABLES

LIST OF FIGURES

Figure Page

CHAPTER 1

INTRODUCTION

In the search for physics beyond the Standard Model, high precision experiments to measure fundamental properties of particles are an important frontier for future research. One area of importance is the measurement of magnetic dipole moment (MDM) values as well as searching for an electric dipole moment (EDM).

For these high precision measurements, there is a need for highly precise fields and a highly polarized particle beams with a small momentum spread. Utilizing simulation software allows for the analysis of beam dynamics including properties like the spin of individual particles and the polarization of a beam under highly precise fields for large data sets ($\geq 10^9$ particles). These analyses can then be used to quantify correlations between phase space variables and spin, giving insights into experimental results as well as methods for optimizing controls.

Fortuitous timing allowed for performing this analysis in conjunction with Fermilab's Muon g-2 experiment, which required analyzing how to maintain a highly polarized beam of muons and determining the effects of correlations among phase space variables. This experiment also attempts to search for an EDM for the muon as part of its overall mission for measuring the anomalous magnetic moment.

1.1 Why is this important?

High precision experiments require an understanding of how phase space variables are correlated to the fields they encounter and how those correlations can be mitigated or controlled via experimental means. With these types of experiments at the forefront of the search for beyond Standard Model physics, analysis of beam dynamics is paramount to understanding how to achieve high precision experimental results by understanding statistical uncertainties.

1.2 Magnetic Dipole Moments and Electric Dipole searches of Muons

Muons have been a particle of choice for these types of analyses because creating highly polarized muon beam, as well as measuring the precession of its spin can be done to a remarkable accuracy, due to the way that muons are both created and how they decay. The muon system can also be described very accurately by the Standard Model of particle physics, thus providing a very accurate comparison between theory and experiment.

Classically, the magnetic dipole moment can be pictured by imagining that our particle is simply a rotating charged sphere. The rotation of charge acts like a current in a loop of wire, and provides the source for a magnetic dipole. The dipole moment, then, is simply a measure of how much this dipole term will interact with an external field.

An electric dipole is the result of two opposite charges separated by a small distance. With the muon seen as a fundamental particle of the standard model, the presence of an electric dipole moment would indicate the separation of charge inside the muon, and thus

provide indication of constituent particles and the possibility of beyond the Standard Model physics.

For the g-2 experiment, measurement of the MDM requires maintaining a precise field and strongly polarized beam of muons with a small momentum spread. The measurement of the EDM requires understanding effects of stray magnetic fields and how to possibly suppress those effects, including how to potentially optimize a system consisting of E and B fields to enhance signal of an EDM. The optimization of storage ring design for non-zero measurement will be the basis of future work, but here we look for basic spin dynamics through magnetic fields and development of correlations among phase space variables of particle beam in presence of magnetic and electric fields.

A more detailed discussion of the experiment is provided in Chapter 3.

1.2.1 Question: How do Various Beam and Lattice Parameters Affect the Overall Polarization?

A major need of the E989 experiment [1] is a strongly polarized beam of muons, so a delivery system was designed to create this beam for delivery into the g-2 storage ring for measurement.

With high precision experiments, the need to quantify statistical and systematic uncertainties becomes very important. So the purpose of this work is to find out which properties of the beam and the lattice (the arrangement of focusing elements) have the greatest impact on the overall polarization of the beam.

We'll examine how the beam emittance, magnet lattice misalignment, and momentum spread all play into the overall spreading of the individual particle spins in the beam, and how that can be represented as a spread in the overall polarization of the beam itself.

CHAPTER 2

ACCELERATOR PHYSICS

2.1 Introduction

In the most basic terms, accelerator science deals with transportation of particles from a source to a target. Though it may be easy to state the nature of the field, it is important to note that it provokes more questions than answers. How should the particles be transported? Do they need to arrive continuously or in bunches? Is the target fixed? What energy do they need? Questions such as these are simply a jumping off point, but serve as a good indicator of the types of experimental conditions an accelerator physicist needs to consider.

It's worth noting that the need to focus this work for a seasoned audience conflicts with the author's desire to make it as self-containing as possible. To resolve this, the technical details of the derivations in this chapter are left as an appendix, so a novice reader can fill in the gaps.

We begin with a problem common to first-year physics students: the motion of a charged particle under the influence of electic and magnetic fields. To solve this problem, we can use the Lorentz force equation

$$\vec{F} = q\vec{E} + q\vec{v} \times \vec{B} \tag{2.1}$$

Our goal is to find a way to transport a beam of particles, knowing we have the option of using electric or magnetic (or both) fields. It's clear to see that a highly relativistic particle

can receive a strong force with only a small magnetic field, but an equivalent force due solely to an electric field would require a significantly stronger electric field.

It is for this reason that accelerators utilize magnetic fields to manipulate beams of particles by steering and focusing them.

We also note Maxwell's equations in media

$$\nabla \cdot \vec{D} = \rho_{free} \tag{2.2}$$

$$\nabla \times \vec{E} = -\frac{\partial \vec{B}}{\partial t} \tag{2.3}$$

$$\nabla \cdot \vec{B} = 0 \tag{2.4}$$

$$\nabla \times \vec{H} = \vec{j}_{free} + \Big(\frac{\partial \vec{D}}{\partial t}\Big) \tag{2.5}$$

Also needed are the equations of special relativity, which describe the behavior of particles as their velocities approach the speed of light ($c = 2.98 \times 10^8$ m/s). Two important parameters we will use in our relativistic equations are β and γ, which are defined below.

$$\beta = \frac{v}{c} \tag{2.6}$$

$$\gamma = \frac{1}{\sqrt{1-\beta^2}} \tag{2.7}$$

Having completed a basic reminder of the relevant equations, we turn our attention to building the necessary blocks for defining a beam lattice.

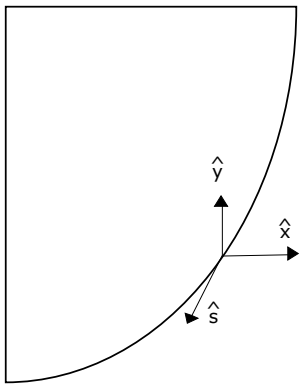

Figure 2.1: The figure above shows a right-handed coordinate system where $\hat{s}$ is coordinate along the curved path of motion. The $\hat{x}$ and $\hat{y}$ coordinates represent transverse motion.

2.1.1 Coordinate System

An objective we must complete is to define a consistent coordinate system with which we can describe our particle in the accelerator. For beams, it's common to use the coordinate system in Figure 2.1 representing a reference particle traveling along an ideal trajectory.

Choosing our coordinates this way allows us to describe the motion of the particle in two separate ways. Longitudinal motion, which is the motion along the $\hat{s}$ direction, and transverse motion, which is motion in the $\hat{x}$ and $\hat{y}$ directions. The $\hat{x}$ direction corresponds to motion in the horizontal plane of the reference particle, while the $\hat{y}$ direction corresponds to motion in the vertical plane.

It is important to note at this point that it's much simpler to imagine the case of an ideal particle, which travels along the $\hat{s}$ vector as it moves, and then describe the motion of all other particles *relative* to that particle's trajectory.

This often allows us to simplify the complications of working in a global coordinate system.

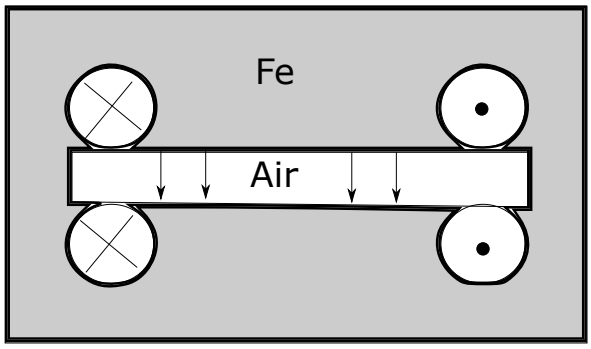

Figure 2.2: The figure above shows the interior cross-section of a dipole magnet, wherein current carrying wire is represented by the circles. The current creates a magnetic field downward in the empty cavity (Air) region in the iron.

2.1.2 The Bending Magnet

The objective of accelerators is to guide a beam of particles along a certain trajectory in the longitudinal direction. As noted before, the easiest way to accomplish this for highly relativistic particles is to utilize magnetic fields. Using Figure 2.2 as an example, we can imagine a charged particle traveling in the $\hat{s}$ direction (into the page). The magnetic field is oriented in the $-\hat{y}$ direction (down) and thus causes the particle to deflect in the $\hat{x}$ direction (to the left).

For a charged particle, the presence of a uniform magnetic field oriented in the positive (or negative) $\hat{y}$ direction would result in uniform circular motion. The radius of this motion is proportional to the velocity, so the area of the field needed is proportional to the velocity of the particle.

Creating a magnetic field large enough to completely enclose an accelerator ring is both costly and impractical. Instead, bending (dipole) magnets create a uniform magnetic field which forces the charged particle to bend over a certain angle.

They are then placed strategically throughout the accelerator in order to manipulate a particle along the desired trajectory. Figure 2.2 illustrates a dipole magnet.

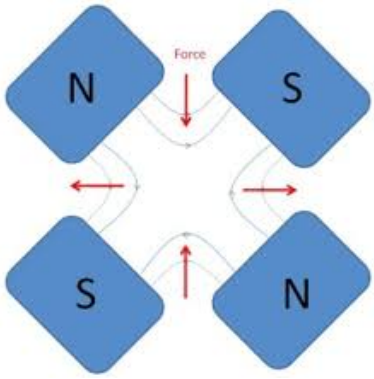

Figure 2.3: The figure above shows the cross section of a quadrupole magnet. The blue arrows represent the direction of the magnetic field lines. The red arrows represent the direction of the force experienced by the a positively charged particle traveling into the page.

Though we've established how a particle can be steered using magnets, we must (momentarily) leave the realm of single particles and instead, imagine a system of more than one particle.

2.1.3 The Focusing Magnet

Imagine for a moment two particles with a given position and momentum, ignoring any Coulomb forces between the particles. As they travel along the $\hat{s}$ direction, they may first move either toward or away from each other (depending on the direction of their initial momenta). But when we think of the long-term behavior of these particles, they will inevitably drift apart. This ultimately causes problems for experimenters hoping to see the effects of particle collisions either with a fixed target or another beam. So we must find a way to keep our particles from drifting apart. This is accomplished with a focusing magnet.

A focusing magnet utilizes a quadrupole alignment (see figure 2.3) of magnetic poles. The benefit is that this particular arrangement of poles creates a magnetic field which will

redirect the motion of a particle which deviates from the ideal trajectory. We'll take a moment to explain the mathematics of how this is possible.

Using Maxwell's equations and noting that our magnet is designed such that there is no free current ($J = 0$) and no electric field ($\vec{E} = 0$), we are able to write equation 2.5 as

$$\nabla \times \vec{B} = 0 \tag{2.8}$$

In order for this identity to hold, we know that all components of $\vec{B}$ must vanish simultaneously. Let's take a look at the $\hat{s}$ component as an example. We have

$$\nabla \times \vec{B}_s = \Big(\frac{\partial B_y}{\partial x} - \frac{\partial B_x}{\partial y}\Big)\hat{s} \tag{2.9}$$

We can define two gradient terms, and note that they are

$$B'_y = \frac{\partial B_y}{\partial x} \tag{2.10}$$

$$B'_x = \frac{\partial B_x}{\partial y} \tag{2.11}$$

We desire a linearly proportional field. That is, particles futher from the ideal trajectory receive a stronger kick than those which are closer to the ideal trajectory. Figure 2.4 shows how the field varies with x position for a hypothetical magnet. But the need for these two gradients to add to zero means that we can only focus in one direction at a time. The solution to this problem is to alternate the magnets so they focus in one plane and then defocus in the same plane. Edwards and Syphers have shown that by choosing the magnet field strengths and distances between magnets carefully, it's possible to achieve a net focusing ([2] p.62).

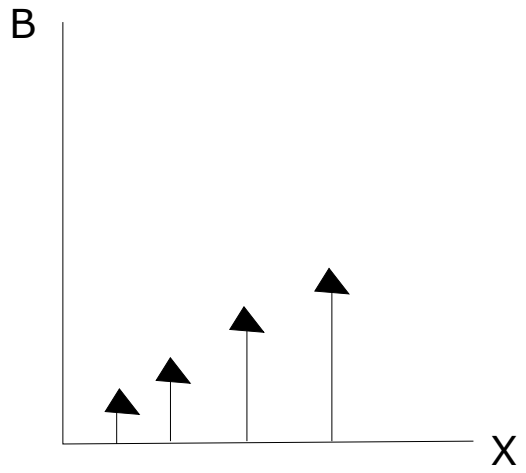

Figure 2.4: The figure above shows the desired field strength at various x positions.

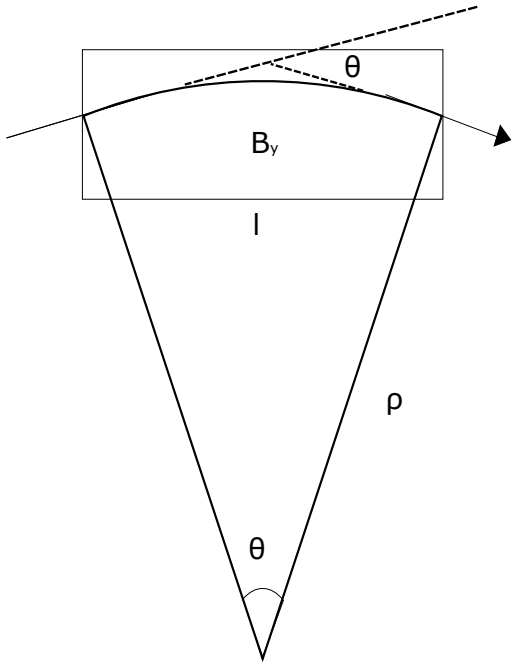

Figure 2.5: The figure illustrates a particle entering from the left, following the curved path, and exiting on the right.

Having discussed the nature of the two major magnet types, we remind ourselves of the magnetic ridigity identity

$$(B\rho) = \frac{p}{q} \tag{2.12}$$

The value $(B\rho)$ is referred to as the magnetic rigidity, and is the ratio of a particle's momentum, p to its charge, q. The value for ρ is the radius of curvature and is illustrated in Figure 2.5.

2.2 Transverse equations of motion

Our first task is to define some relations which will become useful later. We want to describe the motion of a particle using Figure 2.6. So we first start with our geometric

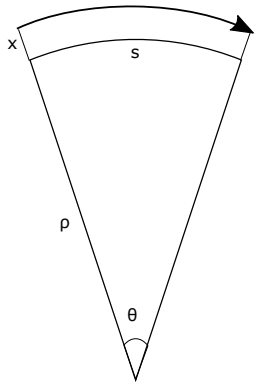

Figure 2.6: The figure illustrates a particle traveling at a displaced value x from the ideal radius ρ.

relation, $\Delta s = \Delta\theta\rho$. But we need a way to relate our unit vectors as well. We remember that $\hat{r}$ is along the path of motion, and $\hat{x}$ is perpendicular to $\hat{s}$ along the radius. This gives the relations

$$\Delta\hat{x} = \Delta\theta\hat{s} \tag{2.13}$$

Now, we can also write our radial position r as the radius of curvature of the ideal particle ρ plus the x position relative to this point

$$r = \rho + x \tag{2.14}$$

We also have our relationship between angular and linear velocity

$$v_s = r\dot{\theta} \tag{2.15}$$

We begin by writing the $\hat{x}$ component of the Lorentz force equation, taking

$$\gamma m(\ddot{r} - r\dot{\theta}^2) = (-qv_sB_y) \tag{2.16}$$

Just as a note, the right hand side only has one component, B_y, because we're assuming the field in the $\hat{s}$ direction is zero. In reality, fringe effects from the wires that protrude at the ends of the magnets do produce fields in the $\hat{s}$ direction.

By looking at our equation, it's clear to see that we have functions of time, which is cumbersome for us. We're going to take advantage of some calculus that allows us to change variables from time to position using the identity

$$\frac{d}{dt} = \frac{ds}{dt}\frac{d}{ds} \tag{2.17}$$

Applying these changes will allow us to get an equation of motion of the form

$$x'' + \left(\frac{1}{\rho^2} + \frac{1}{B\rho}\frac{\partial B_y(s)}{\partial x}\right) x = 0 \tag{2.18}$$

A quick glance shows that this equation generally looks like a one-dimensional harmonic oscillator ($\ddot{x} + k^2 x = 0$) But it's not so simple for us. Our spring constant term is actually a function of position, due to the fact that a particle traveling down a series of beam lattice is focused and steered based on the magnetic fields it encounters. Since there is no requirement that these fields be dependent on each other, we're left with a function of the form.

$$x'' + K(s)x = 0 \tag{2.19}$$

This is actually known as a Hill's equation, and we'll invoke periodicity conditions for our beam lattice ($x(s+C) = x(s)$) and use a trial solution with two components, one representing the amplitude change due to the changing magnetic fields along our beam line, and one representing the phase of the oscillation. We guess that our solution is of the form

$$x = Aw(s)\cos(\psi(s) + \delta) \tag{2.20}$$

The $w(s)$ term is an amplitude scaling factor, and $\psi(s)$ is the phase term describing the oscillatory behavior. For the moment, we'll abbreviate our functions by omitting the argument s. Using this form of our solution, we can plug into 2.18 and get

$$x'' + Kx = A(wK + w'' - w\psi'^2)\cos(\psi(s) + \delta) + A(2w'\psi' + w\psi'')\sin(\psi(s) + \delta) \tag{2.21}$$

Since our differential equation is homogeneous, we know that we must find the correct values of A, w (and its derivatives), K, and ψ (and its derivatives) so that the equation equals 0. Obviously, $A = 0$ is a solution, but it's also uninformative. So we turn to our knowledge of trigonometry. There is no value for $\psi + \delta$ for which both cosine and sine will both equal zero, which means the coefficient terms must equal zero simultaneously. We utilize calculus and a constant k, defined as

$$w^2\psi' = k \tag{2.22}$$

and absorbing our phase term into the sine and cosine functions, we're able to formulate a transport matrix which describes how the the values of a particle's x and x' are changed as it moves through a periodic lattice.

2.2.1 Transport Matrices

Building on the results of the previous section, it's possible to write our final equations of motion in matrix form. The large matrix in the equation below is called a transport matrix,

since it acts to transport a particle through a full cycle of a periodic beam lattice from some initial (x, x') coordinates to final (x, x') coordinates.

$$\begin{pmatrix} x \\ x' \end{pmatrix}_{s_0+C} = \begin{pmatrix} \cos(\Delta\psi_C) - \frac{ww'}{k}\sin(\Delta\psi_C) & \frac{w^2}{k}\sin(\Delta\psi_C) \\ -\frac{1+\left(\frac{ww'}{k}\right)^2}{\frac{w^2}{k}}\sin(\Delta\psi_C) & \cos(\Delta\psi_C) + \frac{ww'}{k}\sin(\Delta\psi_C) \end{pmatrix} \begin{pmatrix} x_0 \\ x'_0 \end{pmatrix}_{s_0} \tag{2.23}$$

Where we define the term ψ as the phase advance of the oscillation, defined as

$$\psi(s_0 \to s_0 + C) \equiv \Delta\psi_C = \int_{s_0}^{s_0+C} \frac{k}{w^2(s)} ds \tag{2.24}$$

and s_0 can be any arbitrary point on the periodic lattice. While this transport is helpful, it still limits us to transport across a single period, C. A more general approach which allows us to transport between any two points on a beamline lattice utilizes the work of Courant and Snyder [3], who noted that the following transformations

$$\beta(s) = \frac{w^2(s)}{k} \tag{2.25}$$

$$\alpha(s) = -\frac{1}{2}\left(\frac{d\beta(s)}{ds}\right) = -\frac{1}{2}\frac{d}{ds}\left(\frac{w^2(s)}{k}\right) \tag{2.26}$$

$$\gamma = \frac{1+\alpha^2}{\beta} \tag{2.27}$$

made it ultimately possible to describe a transport matrix from any point $s_1 \to s_2$ as

$$\begin{pmatrix} x_2 \\ x'_2 \end{pmatrix} = \begin{pmatrix} \left(\frac{\beta_2}{\beta_1}\right)^{1/2}(\cos\Delta\psi + \alpha_1 \sin\Delta\psi) & (\beta_1\beta_2)^{1/2}\sin\Delta\psi \\ -\frac{1+\alpha_1\alpha_2}{(\beta_1\beta_2)^{1/2}} + \frac{1-\alpha_1\alpha_2}{(\beta_1\beta_2)^{1/2}}\cos\Delta\psi & \left(\frac{\beta_1}{\beta_2}\right)^{1/2}(\cos\Delta\psi - \alpha_1\sin\Delta\psi) \end{pmatrix} \begin{pmatrix} x_1 \\ x'_1 \end{pmatrix} \tag{2.28}$$

This serves as a powerful tool which allows only the knowledge of initial conditions (x_1, x'_1), the β function for the entire lattice, and the phase difference between any two points on the

lattice in order to determine the trajectory (x_2, x_2') at a final point. We have one final piece of our puzzle to address before the foundation is set.

2.3 Beam Properties

We can begin by writing our solution to Hill's equation for some arbitrary position along our beam lattice, omitting the argument s from our ψ and β functions, though remembering that they are still both functions of s.

$$x = A\sqrt{\beta}\cos(\psi + \delta) \tag{2.29}$$

Now, if we were to take the derivative of x, we would have

$$x' = -A\psi'\sqrt{\beta}\sin(\psi + \delta) + \frac{1}{2}A(\sqrt{\beta})^{-1}\beta'\cos(\psi + \delta) \tag{2.30}$$

Since our x component contains a cosine function, and our x' component contains a sine function, it would be nice to find a way to transform one of them in order to end up with the equation of a circle. Thankfully, we can utilize the transformation

$$\alpha x + \beta x' = b \tag{2.31}$$

to eliminate the cosine term in equation 2.30 and get

$$\alpha x = \left(-\frac{1}{2}\right)\beta' A\sqrt{\beta}\cos(\psi+\delta) \tag{2.32}$$

$$\beta x' = \beta\left(-A\psi'\sqrt{\beta}\sin(\psi+\delta) + \frac{1}{2}A(\sqrt{\beta})^{-1}\beta'\cos(\psi+\delta)\right) \tag{2.33}$$

$$\alpha x + \beta x' = -A\sqrt{\beta^3}\psi'\sin(\psi+\delta) - \frac{1}{2}\beta' A\sqrt{\beta}\cos(\psi+\delta) + \frac{1}{2}\beta' A\sqrt{\beta}\cos(\psi+\delta) \tag{2.34}$$

It's clear the cosine terms cancel upon addition, and since we defined our phase advance such that

$$\psi(s_1 \to s_2) = \int_{s_1}^{s_2} \frac{ds}{\beta(s)} \tag{2.35}$$

It's clear to see $\psi' = 1/\beta$, and we're left with

$$\alpha x + \beta x' = -A\sqrt{\beta}\psi'\sin(\psi+\delta) \tag{2.36}$$

Now we can plot a particle on a transformed a and b axis as a circle with radius

$$r = A\sqrt{\beta} \tag{2.37}$$

If we square equations 2.29 and 2.36 and add them together then utilize our Courant-Snyder definitions, we would have

$$A^2 = \gamma x^2 + 2\alpha x x' + \beta x'^2 \tag{2.38}$$

We've spent a lot more time on this than the other derivations because it shows that there is some invariant value, A^2, that does not depend on the location of the particle along the lattice. So let us take a moment to think of a single point on a periodic lattice. If the phase advance is irrational, each time the particle returns to some location, it would appear at some different point on its own circle of radius $A\sqrt{\beta}$. If we extend this argument to many

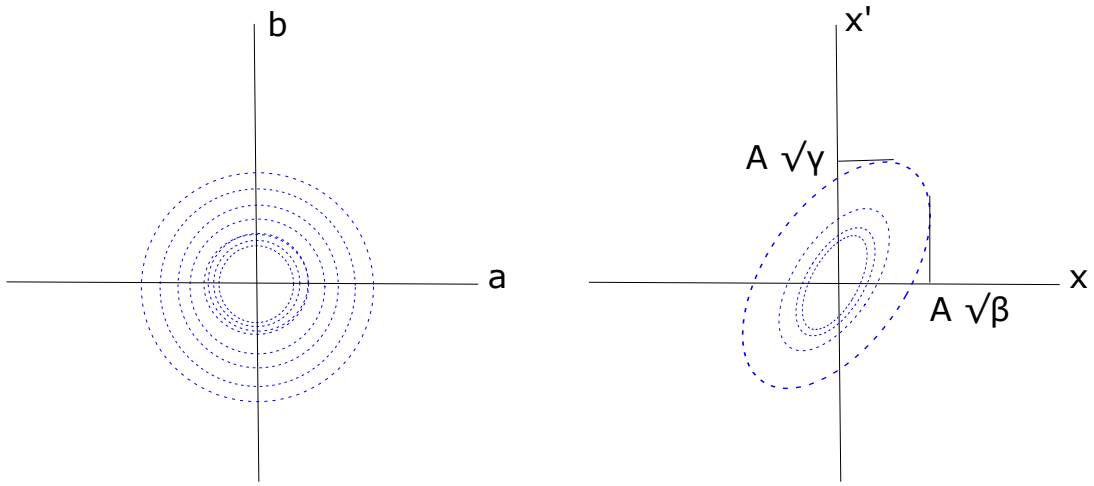

Figure 2.7: The figures above show the locations of particles through a periodic lattice, as they return to an arbitrary value of s. On the left, the plot is in transformed space, $a = x$ and $b = \alpha x + \beta x'$. On the right, a traditional phase space plot, with the maximum values of x and x' noted in terms of their Courant-Snyder variables and A.

particles, we could see that each would trace out a circle of its own radius $A_i\sqrt{\beta}$. It's possible to show that this invariant value is proportional to the area of the phase space, scaled by a factor of π, such that the area of the phase space, (x, x'), is πA^2. The area of the phase space is known as the emittance (denoted ϵ) of the beam, and can be given in various forms. The one we'll most commonly use is the root mean square (RMS) emittance, which contains the particles within $\pm 1\sigma$ of the center, which is about 40% of the particles in the beam. We should also note a subtle distinction that the transformed space, (a, b), does not have a fixed area throughout the beam lattice. Instead, the area of the circle scales with the β along the beam line.

Now that we have a relationship that relates the emittance parameters x and x' to the β and γ values, respectively, it is clear that the beam lattice dictates the behavior of the particles in the beam, and as we saw above, it also describes the shape of the beam itself. Propagation of a beam envelope will depend upon the initial distribution of particle trajectories in phase space. Because the beam behavior through the lattice is dependent on

those initial conditions, it becomes important to design a beam lattice that produces a beam with the right β and α at some target.

As noted, the actual emittance of a beam takes the shape of an ellipse, but we can transform our emittance to a circular shape using the transformation noted in 2.7. For the purposes of simulations, it becomes a simple task generate a distribution of particles with specific β and α values in order to match the needs of our lattice.

A large portion of the simulation work in chapter 4 relied upon this property to develop samples of particles which match certain lattice parameters. The general approach was draw a random number with a standard deviation of 0.001-0.005, which would serve as the x or b variable. Then, using the desired $b = \alpha x + \beta x'$, we transform our random b value into a slope (or momentum, if multiplied by the total momentum of the particle)

$$x' = \frac{b_{rand} - \alpha x_{rand}}{\beta} \tag{2.39}$$

Where the subscript *rand* denotes the randomly drawn values. Since the emittance of the beam is dependent on the position and slope values of the particles within the beams, we can define some statistical relationships between the properties of the beam, the Courant-Snyder values, and the emittance.

$$\beta = \frac{\pi\sigma_x^2}{\epsilon} \tag{2.40}$$

$$\gamma = \frac{\pi\sigma_{x'}^2}{\epsilon} \tag{2.41}$$

$$\alpha = -\frac{\pi\sigma_x\sigma_{x'}}{\epsilon} \tag{2.42}$$

As mentioned above, the desire to produce a beam that matches specific β and α values at some point means we ultimately desire a collection of particles with certain statistical properties.

Having completed our review of beam optics, we can turn our attention to the test case for our analysis, the Muon g-2 experiment.

CHAPTER 3

THE G-2 EXPERIMENT

The g-2 experiment aims to measure the anomalous magnetic moment of the muon by tracking muon decays as the beam circulates around a storage ring under the influence of a highly uniform magnetic field. This chapter examines the reason for the choice of the muon and explains the underlying physics of spin behavior in electric and magnetic fields.

3.1 The Muon

The discovery of the muon was a consequence of the search for the mediator of a strong force which binds the nucleus together. Classically, there's no explanation for why protons could maintain stability in a nucleus despite overwhelming repulsive Coulomb forces.

Hideki Yukawa [4] had formulated the existence of a field which confines protons and neutrons in the nucleus, and a search began to identify the particles which mediate this force, now known as the strong force. Kunze [5], in an experiment using a Wilson cloud chamber, had photographed a yet unknown particle, though its exact nature remained uncertain. In the race to find Yukawa's particle, Anderson [6] and Neddermeyer [7] confirmed the existence of a particle in cosmic rays which had a mass between that of an electron and a proton, which would have fit the track that Kunze photographed. These results were confirmed by Street and Stephenson [8], Nishina, Tekeuchi, and Ichimiya [9], and also by Crussard and Leprince-Ringuet [10]. While this new particle did not end up being Yukawa's strong force mediator, it was however, quite important, since it was a second generation lepton, with a mass of

105 MeV and a mean lifetime of 2.2 μs. This particle was later named the muon, and it had two interesting properties regarding its creation and decay. Muons created from pion decays have a spin vector in the direction of the velocity, and decay with an electron in the opposite direction of the spin. Both of these properties allow it to be an ideal candidate for high precision experiments.

3.2 Spin Precession in a Magnetic Field

Classically, spin can be pictured by treating a particle as a charged sphere which is actually spinning, where the current due to the moving charge induces a magnetic dipole moment. While the classical picture gives us some intuition of spin, it is ultimately a quantum mechanical property, and explained as an intrinsic angular momentum of the charged particle. In the case of the muon, a spin 1/2 particle, it has two possible spin states, $\pm 1/2$. But what does spin 1/2 mean about the direction of the spin? The nature of quantum mechanics forces us to think in terms of probabilities, thus we can define the spin along a particular axis, say S_x, as the expectation of the measured value for spin if a detector was placed along the x axis. By doing this along the x, y, and z axis, we should be able to define a vector for spin as

$$\vec{S} = \ < S_x > \hat{x} \ + \ < S_y > \hat{y} \ + \ < S_z > \hat{z} \tag{3.1}$$

While quantum uncertainty forbids us from measuring S_x, S_y, and S_z at the same time, this spin vector does have a few powerful consequences. First, the sum of the squared expectation values for each axis is one. Second, if we extend our analogy of spin to an ensemble of particles, like a beam, we can say the spin vector represents the location a detector would need to be placed in order to have a maximum probability of detecting every

particle in the beam. Finally, we can treat the spin vector as a representation of the axis of rotation, which conveniently acts as the magnetic dipole vector.

When a magnetic dipole enters a magnetic field, it experiences a torque, represented by

$$\vec{\tau} = \vec{\mu} \times \vec{B} \tag{3.2}$$

which causes the dipole to want to align in the direction of the field. In this, $\vec{\tau}$ is the torque, $\vec{\mu}$ is the magnetic dipole moment and $\vec{B}$ is the magnetic field. This results in a precession of the dipole moment around the direction of the field.

Turning our attention to the muon, it has a magnetic moment determined by the equation

$$\vec{\mu} = g\left(\frac{Qe}{2mc}\right)\vec{s} \tag{3.3}$$

where g represents the g-factor, e is the fundamental charge, m is the mass, c is the speed of light in vacuum, and $\vec{s}$ denotes the orientation of the spin vector. The factor Q is simply ± 1 depending on the charge for the muon.

When special relativity was added to quantum mechanics by Dirac, he formulated that the interaction of a charged particle with an electromagnetic field would give a g-factor of 2 [11]. However, experiments on muons by CERN in the 1960s [12] found that for muons, $g = 2(1 + a)$, where a is the anomalous magnetic moment. The consequence of this small difference is profound, since it indicates the existence of new physics which the Standard Model should be able to explain. However, second order estimates using the standard model still have a 2.2 to 2.7 σ discrepancy [13] between the theoretical and experimental values.

Hyaving discussed the relationship between spin and our magnetic dipole moment, we wish to describe the motion of the spin of a muon under the influence of electric and magnetic

fields. We can utilize the work of Thomas [14] which was later refined by Bargmann, Michel, & Telegdi [15] giving rise to the Thomas-BMT equation

$$\frac{d\vec{S}}{dt} = \frac{e}{\gamma m}\vec{S} \times \left[(1+a\gamma)\vec{B}_{\perp} + (1+a)\vec{B}_{\parallel} + \left(a\gamma + \frac{\gamma}{\gamma+1}\right)\frac{\vec{E}\times\vec{\beta}}{c}\right] \tag{3.4}$$

which describes how the spin vector (in the particle's rest frame) changes over time under external fields. We note that $\vec{S}$ represents the spin vector, e is the particle's charge, a represents the anomalous magnetic moment factor, β and γ are the relativistic beta and gamma factors, and $\vec{B}_{\parallel}$ and $\vec{B}_{\perp}$ denote the magnetic field components in the longitudinal and transverse directions, respectively. Since the g-2 experiment aims to measure a value for a, let us begin our analytical solution by imagining an ideal case where the motion is always perpendicular to a magnetic field. This allows us to set $\vec{B}_{\parallel} = 0$ and $\vec{E} = 0$. From equation 3.4, then

$$\frac{d\vec{S}}{dt} = \frac{e}{\gamma m}\vec{S} \times (1+a\gamma)\vec{B} \tag{3.5}$$

$$= (1+a\gamma)\frac{e}{\gamma m}\vec{S} \times \vec{B} \tag{3.6}$$

$$\equiv \vec{S} \times \vec{\omega}_s \tag{3.7}$$

For a particle (like a muon) with a single positive or negative charge. If we were to also look at the cyclotron frequency. Starting with

$$\frac{\gamma m v^2}{r} = evB \tag{3.8}$$

allows us to write

$$\vec{\omega_c} = \frac{e}{\gamma m}\vec{B} \tag{3.9}$$

By subtracting $\vec{\omega}_s - \vec{\omega}_c$ we can get an equation that is only dependent on the anomalous magnetic moment.

$$\vec{\omega}_s - \vec{\omega}_c = a\frac{e}{m}\vec{B} \tag{3.10}$$

Where our final result remains dependent on a_μ, the anomalous part of the magnetic moment. By comparing the difference between ω_s and ω_c, we can measure the value of a_μ. However, at this point, we're not quite done. The storage ring in the experiment utilizes electrostatic focusing in the vertical direction, since additional magnetic focusing would interfere with the cyclotron frequency. So we must consider the effects of electric fields, returning those terms the spin frequency ω_s gives the following difference

$$\vec{\omega}_s - \vec{\omega}_c = -\frac{Qe}{m}\left[a_\mu\vec{B} - \left(a_\mu - \left(\frac{mc}{p}\right)^2\right)\frac{\vec{\beta}\times\vec{E}}{c}\right] \tag{3.11}$$

where p is the relativistic momentum of the particle. If we could set the coefficient (term in parentheses) for the $\vec{\beta}\times\vec{E}$ product equal to 0, we could find the "magic" momentum at which this term is 0.

$$a_\mu - \left(\frac{mc}{p}\right)^2 \implies p_{magic} = \frac{m}{\sqrt{a_\mu}} \tag{3.12}$$

which corresponds to a value of 3.094 GeV/c. By operating the storage ring at this momentum, we can reduce the frequency to

$$\vec{\omega}_a = \vec{\omega}_s - \vec{\omega}_c = a_\mu\frac{e\vec{B}}{m} \tag{3.13}$$

This value for the anomalous magnetic moment, a_μ is exactly what the experiment aims to measure. We now turn our attention to the physics of the measurement.

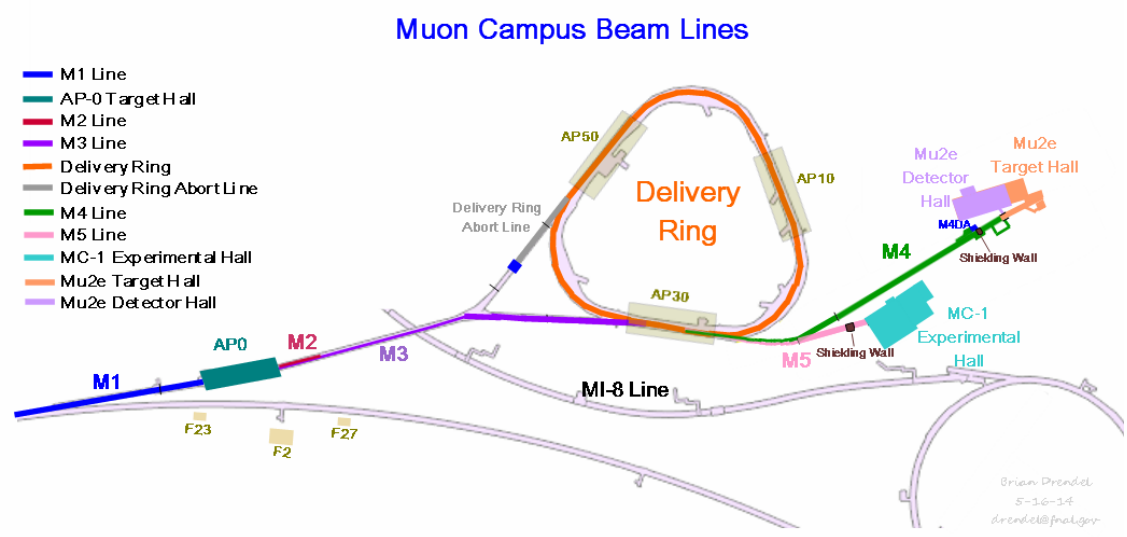

Figure 3.1: The figure above shows the delivery system for the g-2 experiment. A proton beam is transported through M1 into a target at AP0 to create pions. Courtesy Brian Drendel.

3.3 The Experiment

The g-2 experiment requires a proton beam hitting a target and producing protons, pions and a few muons (among other particles) as products of the interactions. These products pass through a bending magnet which helps select those with the magic momentum and are then transported down the M2 and M3 beam lines into the Delivery Ring. The beam makes four turns through the delivery ring to allow the pions to decay into muons before being extracted from the Delivery Ring and transported through the M4 and M5 beam lines to the Storage Ring, where the experiment takes place.

As the pions decay, they preferentially produce muons with spin parallel to the momentum vector. This results in the creation of a strongly polarized muon beam (i.e., the spins of the

individual muons are closely aligned in a common direction). Upon delivery to the storage ring, the muon decays via the weak interaction according to

$$\mu^{\pm} \rightarrow e^{\pm} + \bar{\nu_{\mu}}(\nu_{\mu}) + \nu_{e}(\bar{\nu}_{e}) \tag{3.14}$$

and detectors are positioned to capture the electron tracks. Because the weak decay is parity-violating, electrons preferentially decay antiparellel to the spin of the muon, this allows the experiment to determine which direction the spin orientation was at the time of decay, and in turn, help determine the precession frequency of the muon's spin, ω_a. However, this only works if the spins of all the particles are closely aligned.

3.4 Search for an EDM

While the experiment was specifically designed for a highly accurate measurementt of the MDM, it also allows for a search for an EDM. Physically, the presence of an EDM would manifest itself in an up-and-down oscillation of the decays. Since the experiment uses three tracking stations, the up-and-down oscillations will be detected at two or more orders of magnitude greater sensitivity than has been previously measured ([1] p.78).

Classically, an electric dipole is the result of two opposite charges separated by a distance d. These two charges generate an electric field between them, and the strength of the electric field is proportional to that distance. We can use the principle of superposition to calculate our electric field at the point between the two charges as

$$\vec{E} = \frac{2e}{\pi\epsilon_0 d^2}\hat{e} \tag{3.15}$$

Where d is the distance between the charges, e is the magnitude of the charge, ϵ_0 is the permittivity of free space and $\hat{e}$ is a unit vector pointing toward the negative charge. Similarly to the magnetic dipole moment, the electric dipole moment will experience a torque when entering an electric field. The torque is defined by

$$\vec{\tau} = \vec{d} \times \vec{E} \tag{3.16}$$

where $\vec{d}$ represents the electric dipole moment and $\vec{E}$ represents the electric field. We can write our electric dipole moment as

$$\vec{d} = \eta \left(\frac{Qe}{2mc} \right) \vec{s} \tag{3.17}$$

As we can see, the EDM is aligned with the spin similarly to the MDM, and the term η acts in a similar manner to the value of g. While we have come up with a classical example of this dipole moment, it's important to note that at the quantum level, the existence of an EDM is expressly forbidden due to symmetry violations, and would unambiguously provide evidence of new physics.

3.4.1 Symmetry and the EDM

In this section, we'll briefly discuss the three major symmetries explored in high energy physics experiments.

The first symmetry we'll discuss is that of charge conjugation. Simply put, the laws of physics should hold for both a particle and its antiparticle. So if we were to replace all the values for a particle with that of its antiparticle in some equation, we should get the same final result.

Table 3.1: The table illustrates the consequences of sign changes on each term of the Hamiltonian for the parity rules.

Parity Rule \ Term	$\vec{\mu}$	$\vec{B}$	$\vec{d}$	$\vec{E}$
C	-	-	-	-
P	+	+	+	-
T	-	-	-	+

The second symmetry is that of parity, which is spatial reflection. It shouldn't matter if a particle is traveling left to right or right to left in space. By reversing the sign of the position of a particle in space, we should be able to see that the underlying physics remains unchanged.

Finally, time reversal symmetry states that we should be able to either use our initial conditions and propagate a system forward, or take our final conditions and propagate a system "backwards" in time and achieve the same starting conditions.

These are referred to as C, P, and T (respectively) symmetries. It can be shown that Maxwell's equations (in Chapter 2) obey all three symmetries individually, as well as all possible combinations (CP, PT, CT, or CPT).

From quantum mechanics, a spin-$\frac{1}{2}$ particle has a Hamiltonian

$$\mathcal{H} = -\vec{\mu} \cdot \vec{B} + \vec{d} \cdot \vec{E} \tag{3.18}$$

By utilizing our symmetries, we can come up with a table showing the sign of each term in the equation above. By replacing signs in 3.18, we could see that the first term (the magnetic dipole moment portion) is invariant under all symmetries, but the whole Hamiltonian is only invariant for C and CPT symmetries. The discovery of a non-zero EDM would serve as an example of a CP violation.

Now that we've established both the mathematical language of beams and given ourselves some familiarity with the final experiment, it's time to turn our attention to understanding how the spin dynamics of the beam are impacted by transport through the g-2 delivery system.

CHAPTER 4

SIMULATIONS AND RESULTS

As we saw in Chapter 2, it can become quite cumbersome to manually calculate particle trajectories for large numbers of particles in a beam, especially considering that the mathematics didn't include any particle decays or Coulomb forces. This is where we turn to existing computer codes and utilize parallel processing to analyze beam properties. The two computer programs used for analysis were MADx [16] and G4beamline [17]. Since G4beamline handles particle decays and tracks spin (two important capabilities required for the analysis), it was used for the bulk of the work. The analysis was centered on determining the effects of magnetic misalignment in the delivery system of the g-2 experiment. Our delivery system simulation consisted of five parts which were split among two files. The first file contained the M2 and M3 transport lines, which carry the particles from the lithium lens target to the delivery ring, along with the Delivery Ring. The second file contained the M4 and M5 transport lines between the Delivery Ring and the g-2 Storage Ring where the experiment will ultimately take place.

4.1 G4Beamline

For a computer simulation, it is common to define the major elements of the beam lattice, placing them in space along a beamline. The placement is traditionally determined using a reference particle so that the center of the element is aligned with the theoretical

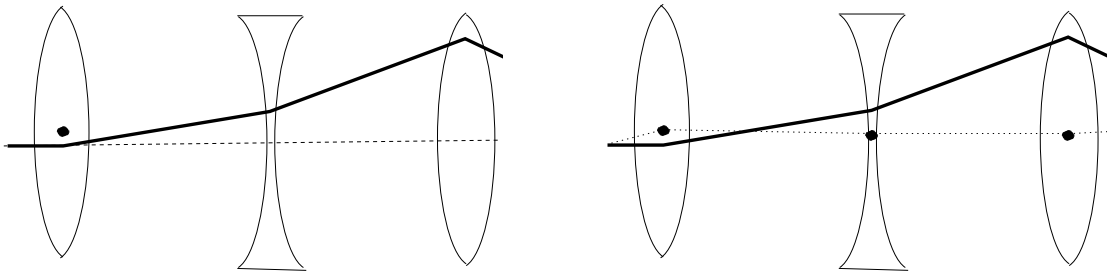

Figure 4.1: The pictures above represent a misaligned focusing quad, where the centers of the magnets are denoted with a dot, and the dashed line represents the reference line $(x, y, s) = (0, 0, s)$ trajectory. Left: Magnet placement for a traditional coordinate system. Right: Magnet placement for a centerline system with a misaligned magnet.

transverse position $(x, y) = 0$. What was discovered about G4Beamline is that it defaults to a centerline coordinate system, which assumes that a lattice element (drift tube, dipole magnet or quadrupole magnet) will always be aligned with the centerpoint of the beam. For analysis interested in the effects of misaligned magnets, this becomes an obstacle, because it couples the magnet position with the beam position.

The left illustration in Figure 4.1, depicts the actual physical effects of a misaligned magnet on a particle's trajectory, which is what we're trying to model. However, the illustration on the right shows G4beamline's centerline coordinate system is defined by the centers of the magnets, whereas we want to have our local coordinate system defined as the ideal design trajectory. The dotted line shows the ideal path for an ideal lattice, in each case. But since the initial magnet was displaced, G4beamline alters the local coordinate system to meet the center of the next magnet, noted by the bend in the dashed trajectory in the figure on the right. This particular nuance of the coordinate system creates an unfortunate problem, but since G4beamline contains the desirable features of particle decays and spin tracking, we wanted to be able to have the capability to analyze the effects of magnet misalignment as well. Fortunately, G4beamline allows for elements to be placed using global fixed coordinates, which remedy this problem, and the careful task of converting existing beamline inputs to global coordinates began.

G4beamline has a survey command that allows a user to get the global coordinates of the front and back of every element in a lattice. Using this command allowed the starting points of all the magnets to be determined, and each magnet could be placed at an (x, y, z) coordinate in real space. The second task became understanding the orientation of each magnet. The M2 and M3 lines experience a slight bend in the $\hat{x} - \hat{s}$ plane and an elevation change in the $\hat{y} - \hat{s}$ plane upon entry to the Delivery Ring. Also, the Delivery Ring is a triangular ring made up of 66 dipoles. Orienting all of these in space required a cumulative tracking of rotation angles of each element with respect to the origin. In some cases, multiple rotations are needed.

If we know the center of the front of the magnet and the rotation angle, we should be able to produce the same coordinates of the back of the magnet. Figure 4.2 shows the results of a comparison for a particle which was tracked using the original centerline lattice as well as the lattice created using global coordinates. The high degree of overlap between the two plots confirms the accurate transformation from centerline to global coordinate systems. So after the lattice was recreated in global coordinates, the same survey command was used to produce an output file and the coordinates were checked against the global coordinates output created from the centerline input file. This was done to excellent accuracy, typically within ± 3 μm, which is several orders of magnitude lower than the range of uncertainties investigated.

Our objective is to displace magnets transverse to the ideal trajectory. But by converting to global coordinates, we cannot simply add the value of the misalignment in the $\hat{x}$ transverse direction to the x coordinate of the placed magnet in real space. The rotation of the lattice element must be taken into account. G4Beamline uses a right-hand rotation rule, meaning that one should imagine gripping the axis of rotation with the right hand, noting the thumb in the positive direction. The way the fingers are curling represents a positive rotation.

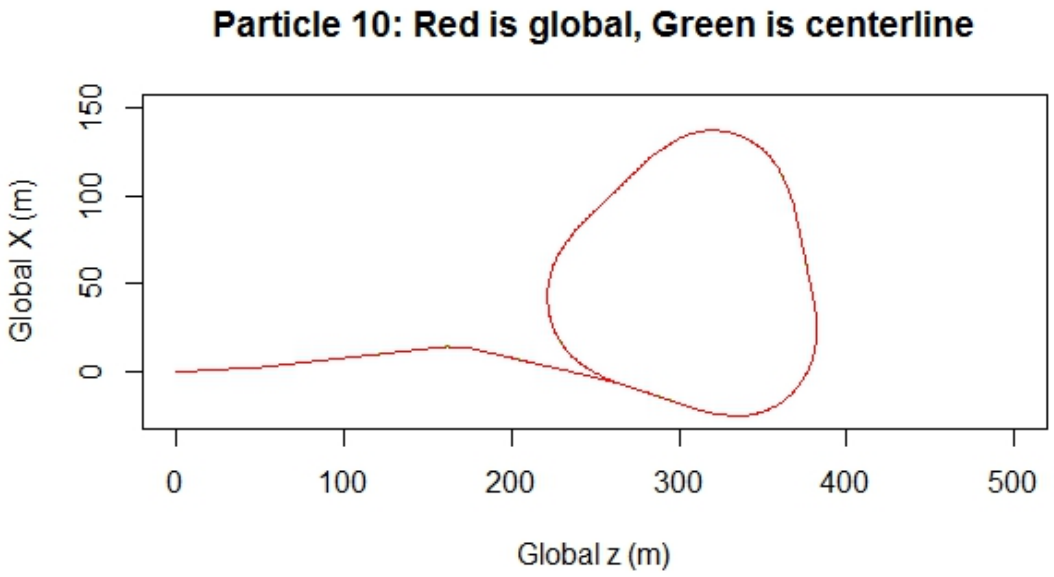

Figure 4.2: The picture above shows particle tracking through a lattice placed using both the centerline and global coordinates have a near-exact match. The survey commands show differences of $\leq \pm 3$ μm.

As we recall from mechanics, we can rotate a vector in rectangular coordinates around an axis by multiplying a rotation matrix by the 3-dimensional coordinate vector. These

rotation matrices are defined below. Note that the subscript on the R represents the axis of rotations, and these matrices represent right-handed rotations.

$$R_x = \begin{bmatrix} 1 & 0 & 0 \\ 0 & \cos(\theta) & -\sin(\theta) \\ 0 & \sin(\theta) & \cos(\theta) \end{bmatrix} \tag{4.1}$$

$$R_y = \begin{bmatrix} \cos(\theta) & 0 & \sin(\theta) \\ 0 & 1 & 0 \\ -\sin(\theta) & 0 & \cos(\theta) \end{bmatrix} \tag{4.2}$$

$$R_z = \begin{bmatrix} \cos(\theta) & \sin(\theta) & 0 \\ -\sin(\theta) & \cos(\theta) & 0 \\ 0 & 0 & 1 \end{bmatrix} \tag{4.3}$$

While other scripts (such as MAD-x) utilize transverse misalignments natively, G4beamline does not. So after completing the process of placing and rotating the lattice elements in space, the need to convert transverse misaligments to global space becomes an issue.

To resolve this problem, a python [18] script was developed that read information from two files. The first file contained a magnet identifier and the x and y transverse displacements and the second file also containing the magnet identifier and the rotations it undergoes in space. The rotations are denoted first by axis then angle. The script used the magnet identifier and combined these two input files, creating an array. Each element in the array was a list containing the magnet name, the x displacement (in the transverse plane), the y displacement (in the transverse plane), and then all the rotations performed on the magnet in space (with a single rotation containing both the axis and angle information).

In order to make it easy to apply these alignment errors, the placement of each element in the beamline was done by adding a parameter value (e.g. `ELEMENT_Xerror`), so the placement command in G4beamline would look something like

```
place ELEMENT   x=0.00+ELEMENT_Xerror    \
y=0.00+ELEMENT_Yerror   z=0.00+ELEMENT_Zerror
```

This would allow for simply defining all the parameters in one section of the input file and make it simpler to load new sets of parameters as misalignment variables changed. Each axis error (e.g. `ELEMENT_Xerror`) corresponded to the results from the multiplication by the rotation matrices.

To verify these rotations, a transverse misaligment was performed in the centerline coordinate system. The survey command once more produced an output file in global coordinates for this misaligment, and the original position (with no misaligment) was compared to see how much the magnet was displaced in the x, y, and z directions. The transverse displacement was also calculated using the rotation matrices in equations 4.1-4.3 and the results matched.

Being able to convert to global coordinates and then also displace transversely in global coordinates eliminates the problem of coupling between the beam and beamline elements brought on by the centerline coordinate system.

4.2 Parameters of Simulations

Ultimately, the goal is determining the sensitivity of the beam's polarization due to magnetic misalignment in the delivery system. Historically, the magnet survey teams at Fermilab have been able to achieve magnet placement precision at the $10^2\mu$m level reliably, so that served as a good benchmark for the scale of the misaligments we analyzed. The

following scenarios were investigated.

1. Simulating misalignments for the M2 and M3 lines, using a root-mean-square (RMS) displacement of 100-1000 μm with a step of 100 μm in either the x or y direction (but not both simultaneously). This was repeated for five sets of random misalignments.

2. Simulating misaligments in both the x and y direction simultaneously on the M2 and M3 lines, with an RMS of 100-500 μm with a step of 100 μm. Each RMS value was repeated for five sets of random misalignments.

3. Simulating misalignments on the Delivery Ring only, with an RMS of 100-500 μm with a step of 100 μm. Each RMS value was repeated for five sets of random misalignments.

An R [19] script generated arrays of displacements in the transverse $\hat{x}$ and $\hat{y}$ directions, based on the RMS needed for the individual trial. Some conditional logic was included to bound the displacements to $\pm 3\sigma$.

During the initial testing phase, the typical sample size was around 500 particles. This was mostly done to limit computational time and served as proof-of-concept for the analysis. The final analysis was done using a statistics file generated using MARS by Korostelev [20], assuming 10^9 protons on target (POT) at the lithium lens.

4.3 Particle Counts

Similar analysis of the effects of misaligment on beam polarization was done by Korostelev [21] on the g-2 project using Bmad [22], which is a code similar to G4Beamline. For most collaborations, doing similar analysis on different codes can help strengthen conclusions (when they agree) or tease out inconsistencies in understanding (when they don't). A first objective was to determine whether sensitivity to misalignments was stronger in one transverse direction or the other.

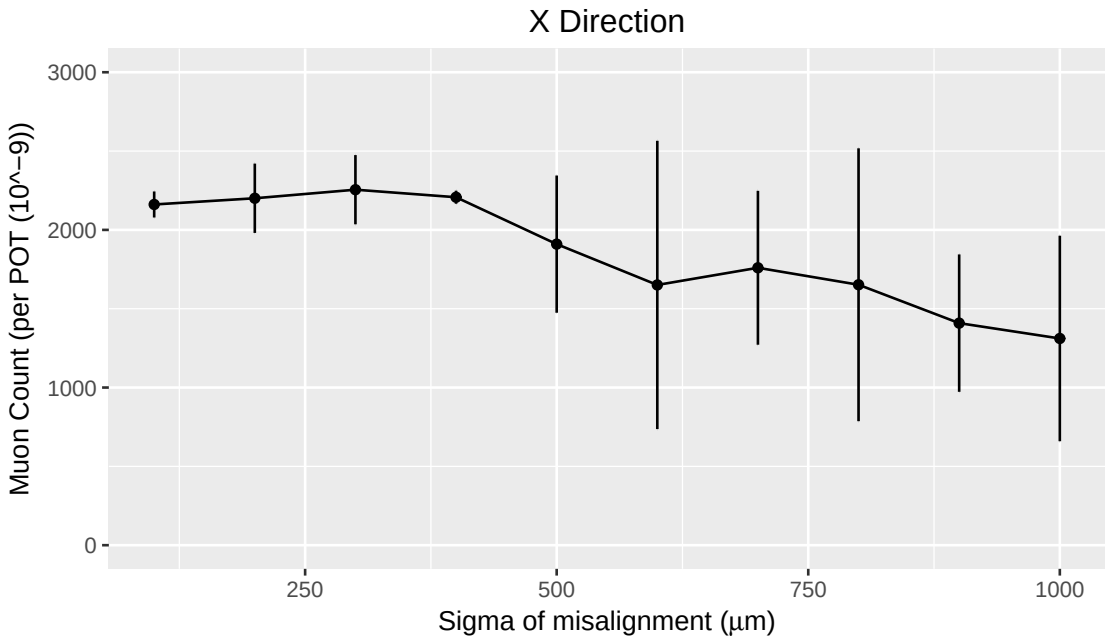

Figure 4.3: Number of Muons after the M2M3 delivery line. The displacements were in the transverse X direction only.

A set of trials used a standard deviation of 100-1000 μm, with a step of 100 μm in the x direction or y direction only. Five sets of random displacements were created for the M2 and M3 beamlines, and the final muon count at the end of the beamline was recorded. Figures 4.3 and 4.4 show the mean (along with 95% confidence intervals) for each displacement standard deviation.

The results for Bmad simulations [21] are shown in figure 4.5. The results show good agreement between Bmad and G4Beamline. This agreement also serves to validate that the transverse misalignment for global coordinates is working correctly using the rotation matrices.

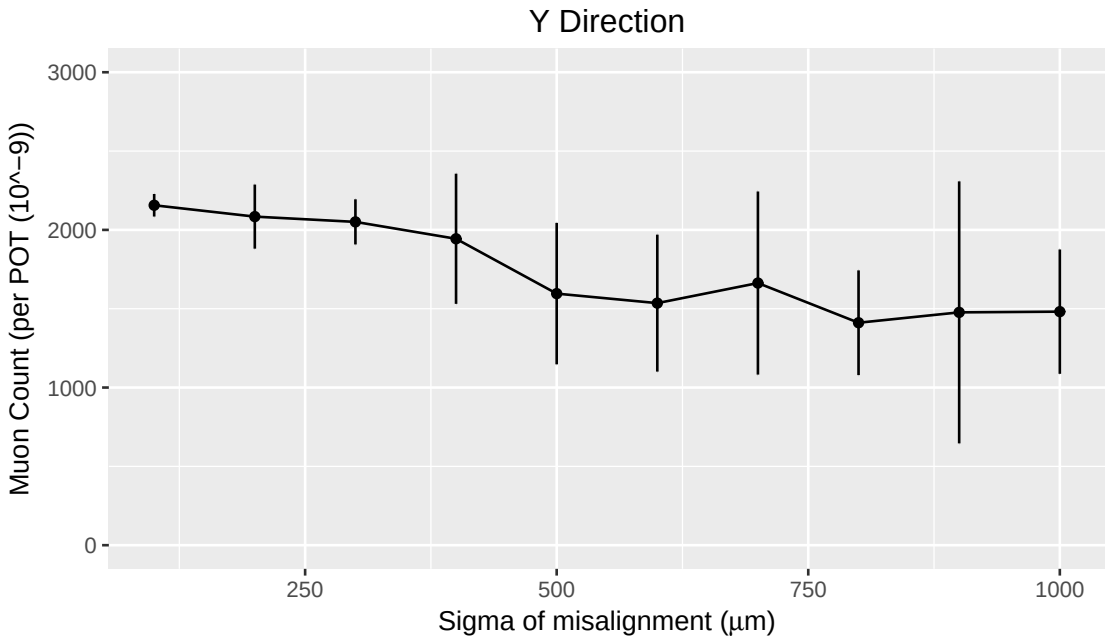

Figure 4.4: Number of Muons after the M2M3 delivery line. The displacements were in the transverse Y direction only.

4.4 Polarization after M2M3 and the Delivery Ring

Though the benefits of using global coordinates were used to misalign magnets in the transverse plane, it's also worth noting that an additional cost was that the global coordinates used for the output files required the use of a transformation from global to local coordinates to determine the spin orientation of the particles in the beam relative to the beam's trajectory. This used the inverse of equations 4.1 - 4.3. These were verified by running a beamline through both centerline and global coordinates and comparing the output of the individual spin components in both coordinate systems. The rotations were then applied to the spin components in global coordinates and compared against the spin components produced in the centerline coordinates, producing a near-exact match.

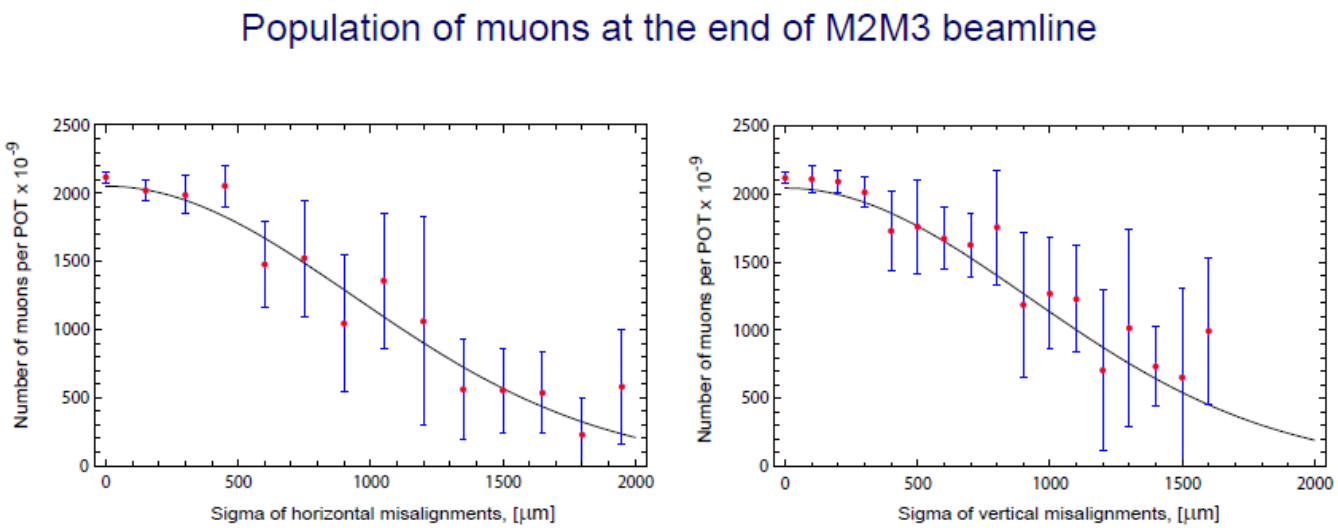

Figure 4.5: Number of Muons after the M2M3 delivery line. The graph on the left denotes displacements in the x direction only, while the graph on the right denotes displacements in the y direction only. These are the results of the Bmad simulations ([21]).

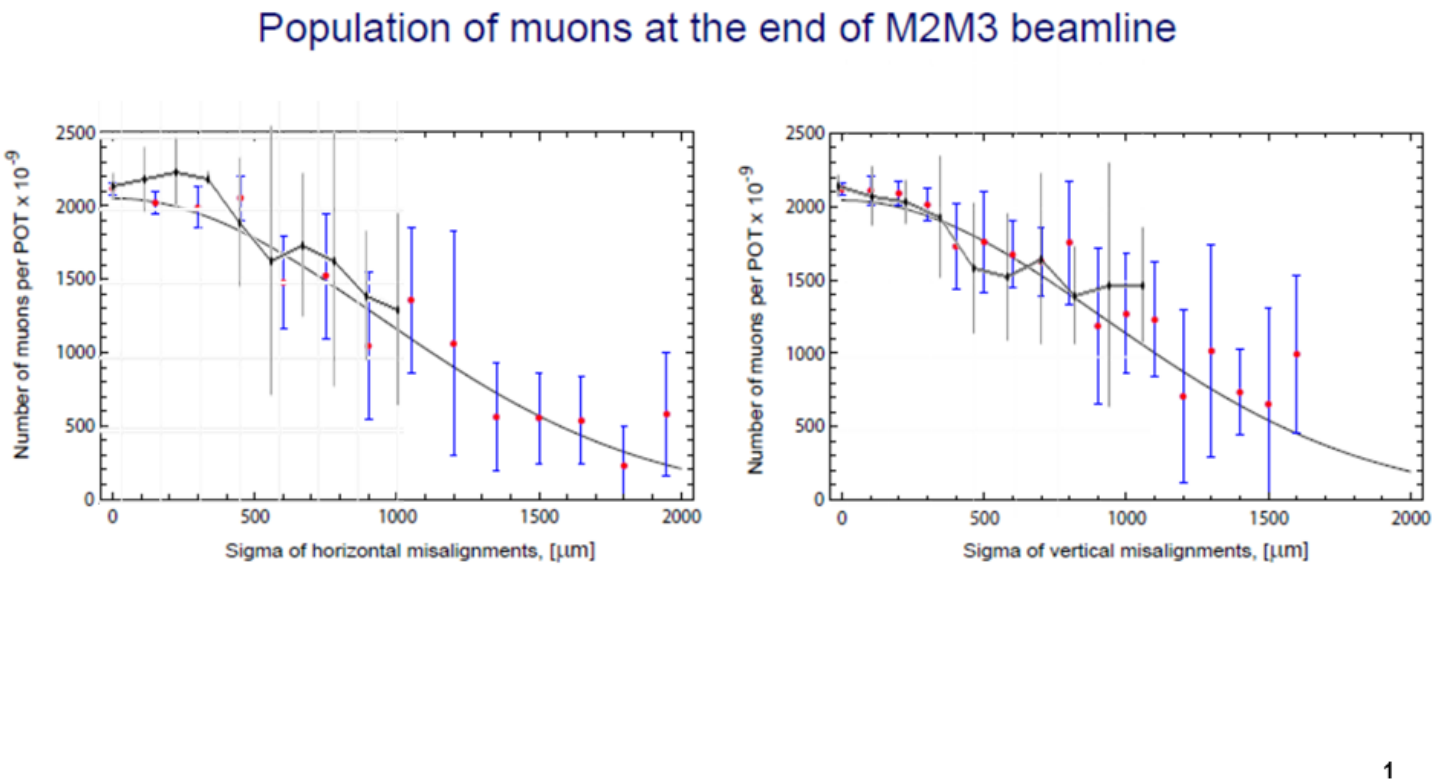

Figure 4.6: This graph shows the comparison between the results from Bmad [21] (the blue lines) and the results of G4Beamline (the black lines), showing a strong agreement of the effects how muon counts are affected by quadrupole misalignments.

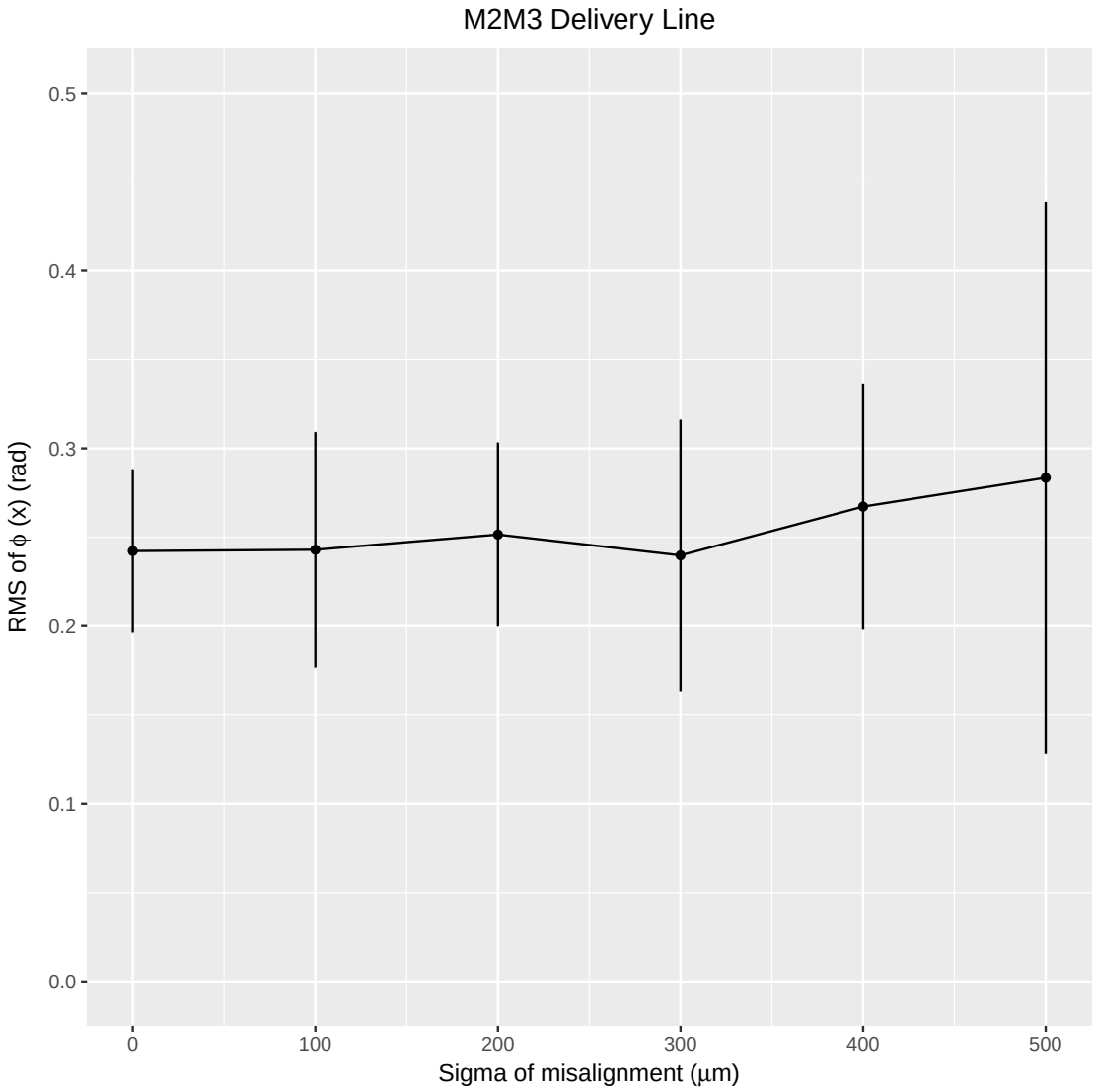

Figure 4.7: Beam polarization in the x direction at end of M2M3 Line.

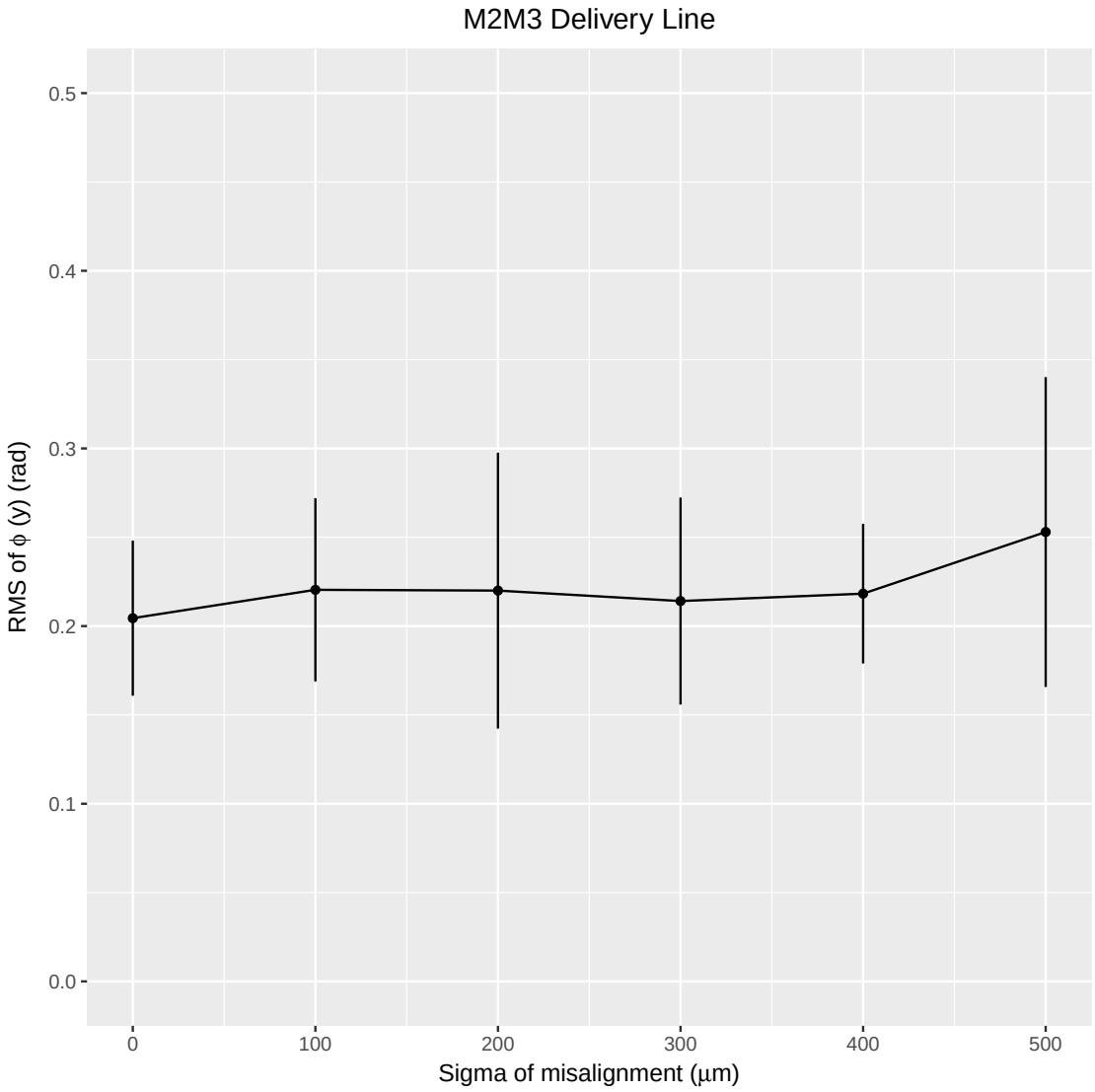

Figure 4.8: Beam polarization in the y direction at end of M2M3 Line.

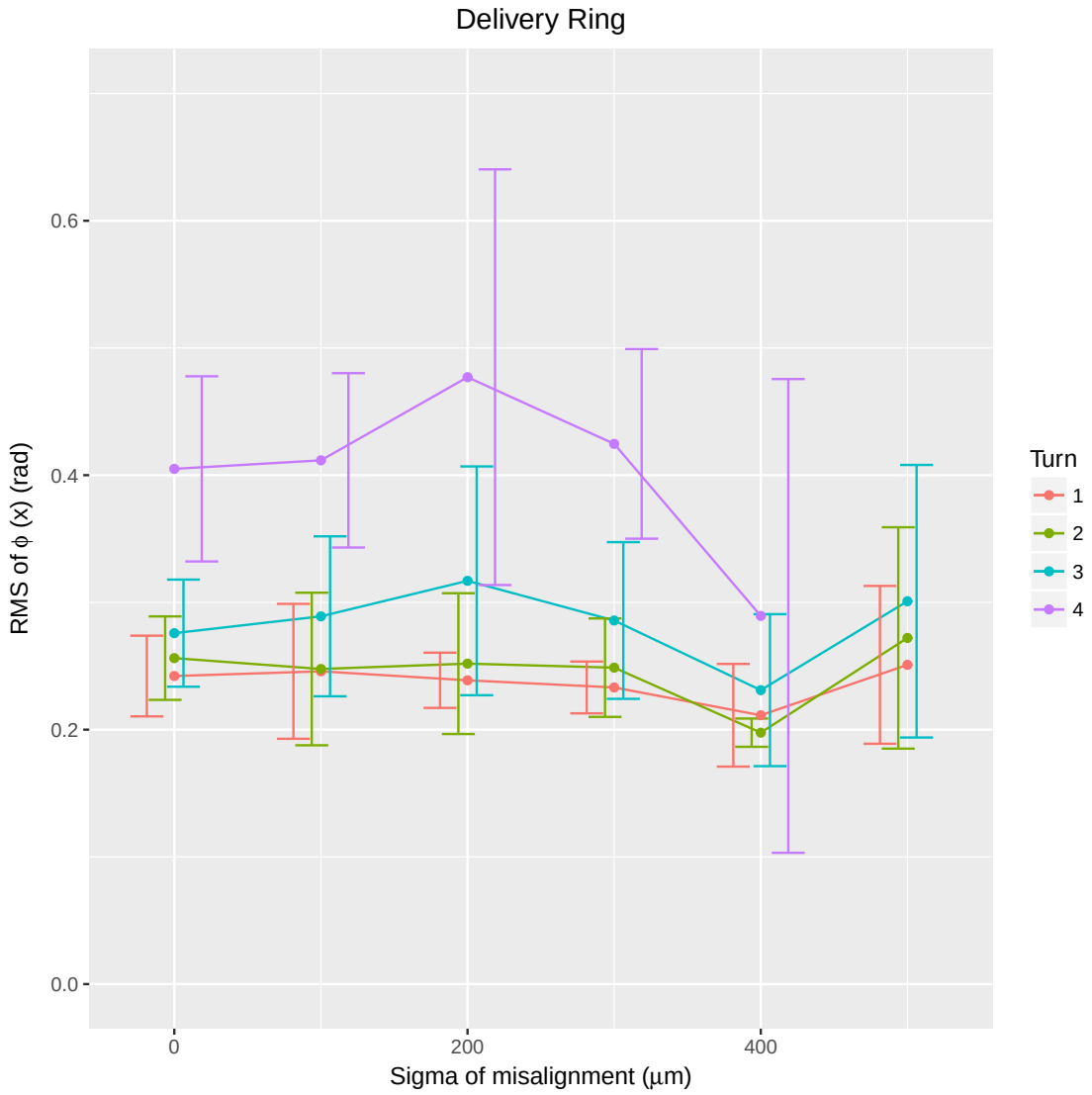

Figure 4.9: Beam polarization in the x direction at end of each turn in the delivery ring.

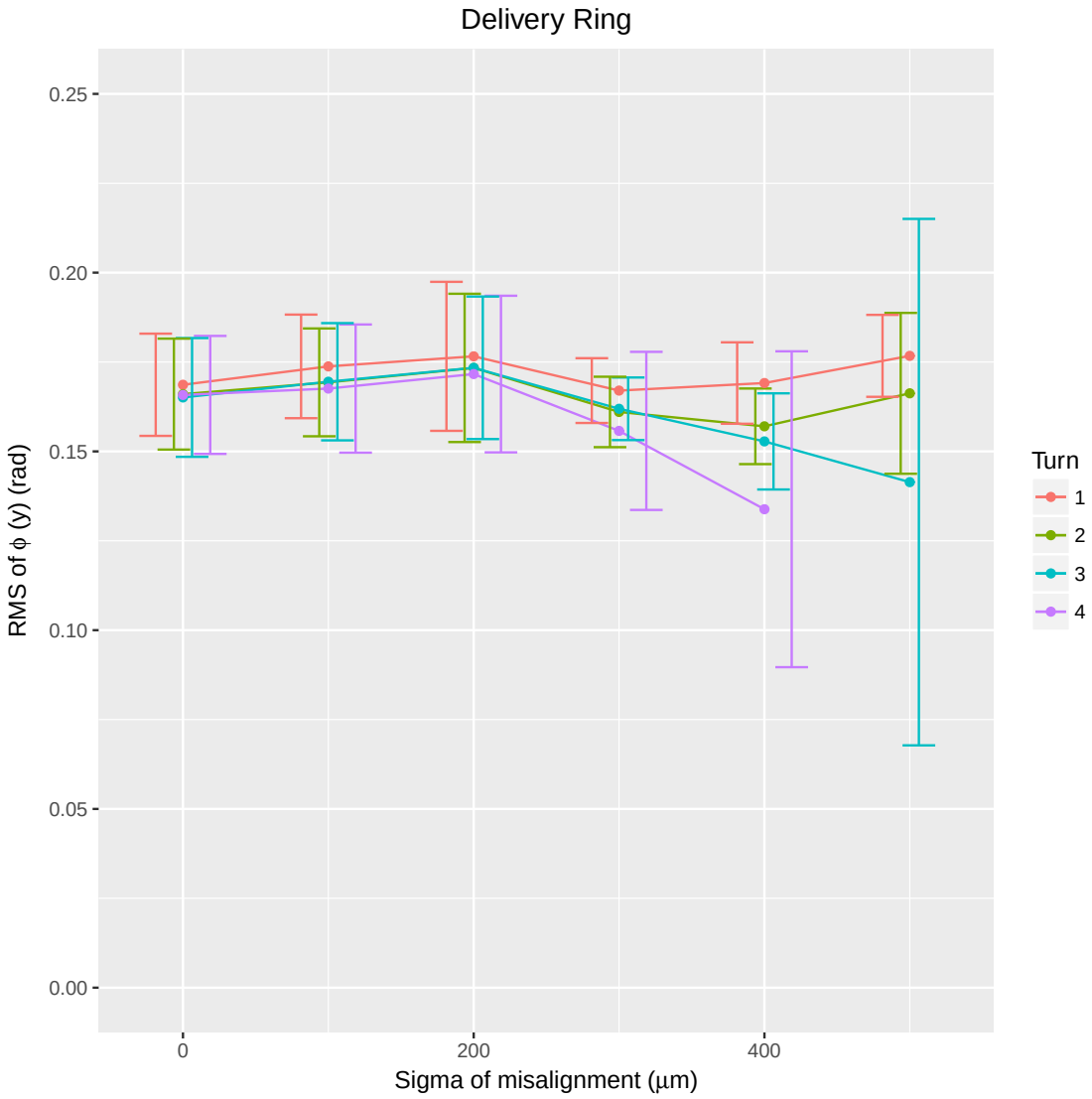

Figure 4.10: Beam polarization in the y direction at end of each turn in the delivery ring.

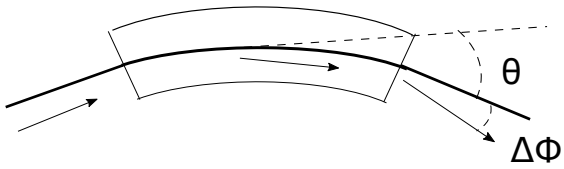

Figure 4.11: The figure above shows a particle with a spin (denoted by the arrows) aligned with the trajectory (the thick line). As the particle enters the bending magnet (with bend angle θ, it encounters a field, and the spin vector precesses by an amount $\Delta\phi$.

In figures 4.7 and 4.8, we can see the polarization of the beam at the end of the M2M3 beamline for the various sigmas of displacements. We shall examine this again analytically later in the chapter.

Figures 4.9 and 4.10 show the beam polarization in the x and y directions at the end of each turn (up to four turns) in the Delivery Ring for a variety of RMS misalignment values. We see essentially no dependence on alignment for the y polarization. In the x direction, we suspect the large jump in polarization for the fourth turn is likely due to a combination of systematic error related to the momentum spread of the beam and a relatively small sample size. This will be examined further later in the chapter.

4.5 Analytical Estimates of Values

While simulation serves as a powerful tool, it is necessary to verify that the results match what is expected analytically. This section provides an overview of the mathematics of spin dynamics for particles, and gives formulas which can be used to verify simulation results. The effects of the main beam and lattice properties on the overall polarization of the beam are looked at in isolation, with the emphasis being the influences of quadrupole magnets.

In order to verify these approximations, Monte Carlo simulations were done and compared these approximations using known values for the M2 and M3 beamlines. It is worth noting that these approximations are done for the x direction, but apply equally as well to y. We

first begin by returning to our bending magnet, illustrated in Figure 4.11. If we imagine a particle whose spin vector is perfectly aligned in the direction of motion, then allow it to pass through a bending magnet, we see that the spin vector, denoted by the arrow, rotates by slightly more than the bending angle, due to precession in the magnet's field. We can describe the change in spin by the formula

$$\Delta\phi = -(1 + a\gamma_r)\theta \tag{4.4}$$

Where the value γ_r is the relativistic gamma factor and a is defined as the anomalous magnetic moment, and was defined in Chapter 3 as

$$a = \frac{g-2}{2} \tag{4.5}$$

Ultimately, we aim to estimate how particle decay, emittance, quadrupole misalignment and momentum spread affect the polarization of the muon beam and by what relative amounts. For our purposes, it is helpful to see how they affect the spread of the spin vectors, so we typically want to determine the spread of the spin due to each effect.

4.5.1 Emittance Effects on Polarization

Knowing our precession contribution from equation 4.4 depends on the particle's change in trajectory θ, we can approximate this angle as the change in slope between two points on the beamline. So our task begins for determining our change in slope between any two points on the lattice.

Recalling from Chapter 2, we can describe the x and x' values for our beam using our Courant-Snyder parameters and the transport matrix in equation 2.28. For convenience in notation, we'll utilize the following definitions

$$a = \left(\frac{\beta_2}{\beta_1}\right)^{1/2} (\cos\Delta\psi + \alpha_1 \sin\Delta\psi) \tag{4.6}$$

$$b = (\beta_1\beta_2)^{1/2} \sin\Delta\psi \tag{4.7}$$

$$c = -\frac{1+\alpha_1\alpha_2}{(\beta_1\beta_2)^{1/2}} + \frac{1-\alpha_1\alpha_2}{(\beta_1\beta_2)^{1/2}} \cos\Delta\psi \tag{4.8}$$

$$d = \left(\frac{\beta_1}{\beta_2}\right)^{1/2} (\cos\Delta\psi - \alpha_1 \sin\Delta\psi) \tag{4.9}$$

This allows us to write the transport matrix as simply

$$\begin{pmatrix} a & b \\ c & d \end{pmatrix} \tag{4.10}$$

Using this notation, we can describe the trajectory of a particle as

$$\begin{pmatrix} x_f \\ x'_f \end{pmatrix} = \begin{pmatrix} a & b \\ c & d \end{pmatrix} \begin{pmatrix} x_i \\ x'_i \end{pmatrix} \tag{4.11}$$

We can make a simple argument that the ultimate contribution to the precession is really just the change in the slope values $x'_f - x'_i$, as is illustrated in Figure 4.12. To find the difference between our initial and final slope values, we use the matrix above and solve for $x'_f - x'_i$.

$$x'_f - x'_0 = cx_0 + dx'_0 - x'_0 \tag{4.12}$$

$$\Delta x' = cx_0 + (d-1)x'_0 \tag{4.13}$$

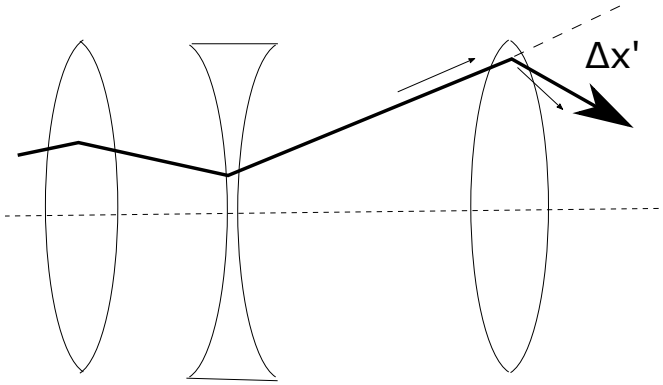

Figure 4.12: The final precession angle is due to the final value for the slope.

Now that we know our value for $\Delta x' = \theta$ we can substitute into equation 4.4 and get

$$\Delta\phi = -(1 + a\gamma_r)\Delta x' \tag{4.14}$$

Our objective remains to find an RMS spread for $\Delta\phi$ so we begin substituting our value for $\Delta x'$ and squaring both sides gives

$$\Delta\phi = -(1 + a\gamma_r)[cx_0 + (d-1)x_0'] \tag{4.15}$$

$$\Delta\phi^2 = (1 + a\gamma_r)^2[c^2x_0^2 + (d-1)^2x_0'^2 + 2c(d-1)x_0x_0'] \tag{4.16}$$

We then average these values over our initial phase space distribution to get

$$< \Delta\phi^2 >= (1 + a\gamma_r)^2[c^2 < x_0^2 > +(d-1)^2 < x'^2_0 > -2c(d-1) < x_0x_0' >] \tag{4.17}$$

We can recall from chapter 2 that we can utilize the substitutions of

$$\frac{\beta_0\epsilon}{\pi} =< x_0^2 > \qquad \frac{\gamma_0\epsilon}{\pi} =< x'^2_0 > \qquad \frac{-\alpha_0\epsilon}{\pi} =< x_0x_0' > \tag{4.18}$$

We can re-write our final RMS value for the change in slope due to emittance as

$$< \Delta\phi^2 > = (1 + a\gamma_r)^2 \left[c^2 \frac{\beta_0 \epsilon_{rms}}{\pi} + (d-1)^2 \frac{\gamma_0 \epsilon_{rms}}{\pi} - 2c(d-1) \frac{\alpha_0 \epsilon_{rms}}{\pi} \right] \tag{4.19}$$

$$\Delta\phi_{rms} = (1 + a\gamma_r) \sqrt{\frac{\epsilon_{rms}}{\pi}} \sqrt{c^2\beta_0 + (d-1)^2\gamma_0 - 2c(d-1)\alpha_0} \tag{4.20}$$

And we have a simple formula that allows us to determine the RMS spread of spin angles due to the emittance of the beam simply by plugging in our Courant-Snyder parameters and our beam emittance, along with the values for c and d.

4.5.1.1 An Alternative Derivation

While this does work out well, it is also wise to remember the transformation we showed in chapter 2, which allows us to turn our elliptical emittance into a circular emittance. The benefit of this will be quite clear in our conclusion. This was achieved via the transformations $a = x$ and $b = \alpha x + \beta x'$. We can begin by noting that we can write our transport matrix for this new coordinate system as

$$\begin{pmatrix} a \\ b \end{pmatrix} = \sqrt{\frac{\beta}{\beta_0}} \begin{pmatrix} \cos\psi & \sin\psi \\ -\sin\psi & \cos\psi \end{pmatrix} \begin{pmatrix} a_0 \\ b_0 \end{pmatrix} \tag{4.21}$$

Since our circular distribution simply rotates in space and is scaled by the ratio of β values as it moves through the lattice (which is illustrated in Figure 4.13). It is worth noting that the value of ψ in the equation above is represented is really the difference in the ψ

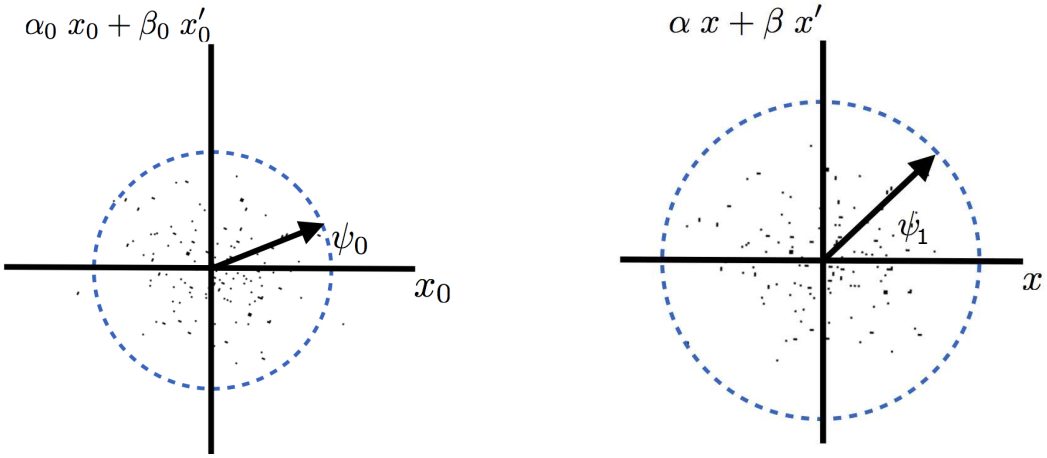

Figure 4.13: The figures above denote the changes in phase for a distribution under the transformation $b = \alpha x + \beta x'$. Under this transformation, the circular distribution rotates (noted by the change in the vector ψ) as the beam traverses the lattice.

values in Figure 4.13, i.e. $\psi = \psi_1 - \psi_0$. Though we want to find our change in slope, $\Delta x'$, we have defined $b = \alpha x + \beta x'$, so instead we are able to write

$$x' = \frac{b - \alpha x}{\beta} \tag{4.22}$$

Noting that equation 4.21 allows us to write

$$b = \sqrt{\frac{\beta}{\beta_0}}(b_0 \cos\psi - a_0 \sin\psi) \tag{4.23}$$

We can now substitute into 4.22 and write

$$x' = \frac{1}{\sqrt{\beta_0\beta}}\left[(b_0 \cos\psi - a_0 \sin\psi) - \alpha(a_0 \cos\psi + b_0 \sin\psi)\right] \tag{4.24}$$

$$= \frac{1}{\sqrt{\beta_0\beta}}\left[-(\sin\psi + \alpha\cos\psi)a_0 + (\cos\psi - \alpha\sin\psi)b_0\right] \tag{4.25}$$

For the sake of brevity in our equations, we'll substitute C for our $\cos\psi$ term and S for our $\sin\psi$ term. This allows us to write, more briefly

$$\Delta x' = x' - x'_0 = \frac{1}{\sqrt{\beta_0\beta}}\left[-(S+\alpha C)a_0 + (C-\alpha S)b_0 - \sqrt{\beta_0\beta}x'_0\right] \tag{4.26}$$

$$= \frac{1}{\sqrt{\beta_0\beta}}\left[-(S+\alpha C)a_0 + (C-\alpha S)b_0 - \sqrt{\frac{\beta}{\beta_0}}(b_0 - \alpha_0 a_0)\right] \tag{4.27}$$

$$= \frac{1}{\sqrt{\beta_0\beta}}\left[-(S+\alpha C - r\alpha_0)a_0 + (C-\alpha S - r)b_0\right] \tag{4.28}$$

Again, for brevity, we utilize $r = \sqrt{\beta/\beta_0}$. We then square both sides to get

$$\Delta x'^2 = \frac{1}{\beta\beta_0}\left[(S+\alpha C - r\alpha_0)^2 a_0^2 + (C-\alpha S - r)^2 b_0^2 - 2(S+\alpha C - r\alpha_0)(C-\alpha S - r)a_0 b_0\right] \tag{4.29}$$

This is where the payoff comes for our distribution. Remember that we chose a and b such that the distribution was circular, and thus, cylindrically symmetric. Because of this, we have $< a_0^2 >=< b_0^2 >$, so when we average our value for $\Delta x'^2$ we can substitute and get

$$< \Delta x'^2 > = \frac{< a_0^2 >}{\beta_0}\frac{1}{\beta}\left[(S+\alpha C - r\alpha_0)^2 + (C-\alpha S - r)^2\right] \tag{4.30}$$

$$= \frac{< a_0^2 >}{\beta_0}\frac{1}{\beta}\left[1 + \alpha^2 - 2r((1+\alpha_0\alpha)C + r^2(1+\alpha_0^2) + 2r(\alpha - \alpha_0)S\right] \tag{4.31}$$

Which we can use our Courant-Snynder definitions to rewrite our result more simply as

$$< \Delta x'^2 >= 2\frac{< a_0^2 >}{\beta_0}\left[\frac{\gamma+\gamma_0}{2} - \frac{1+\alpha_0\alpha}{\sqrt{\beta_0\beta}} + \frac{\alpha-\alpha_0}{\sqrt{\beta_0\beta}}\right] \tag{4.32}$$

We can take advantage of the fact that the leading fraction is simply the definition of emittance (we defined $a = x$ in our transformation, then we can plug the value into 4.4 to get

$$\Delta\phi_{rms} = (1 + a_\mu\gamma_r)\sqrt{\frac{2\epsilon_{rms}}{\pi}}\sqrt{\left[\frac{\gamma + \gamma_0}{2} - \frac{1 + \alpha_0\alpha}{\sqrt{\beta_0\beta}}\cos\psi + \frac{\alpha - \alpha_0}{\sqrt{\beta_0\beta}}\sin\psi\right]} \tag{4.33}$$

For our M2M3 delivery line, we can use this equation to estimate the RMS spin change based on the input parameters, $a \approx 0.001$, $\gamma \approx 30$, $\beta_0 = 2.488$ m, $\beta = 5.0328$ m, $\alpha_0 = 0.175$ & $\alpha = -0.72738$ and an RMS emittance of 7π mm·mrad (assuming a 40π (95%) emittance for a Gaussian beam ([1] p.200)) gives $\Delta\phi_{rms} \approx 2.7$ mrad. Statistical analysis of a sample of 500 muons (with decays turned off) through the M2M3 delivery line gave a value of $\Delta\phi_{rms} \approx 2.8$, which is close to our numeric approximation.

While this equation may seem cumbersome, it does shed some physical insight for a standard FODO cell. This would allow us to condense our final result as

$$\Delta\phi^n_{rms} = 2(1 + a_\mu\gamma_r)\sqrt{\frac{\epsilon_{rms}\gamma_0}{\pi}}|\sin\left(\frac{n\mu}{2}\right)| \tag{4.34}$$

where μ represents the phase advance per cell, and n represents the number of FODO cells. What this is telling us is that the overall spread in spin angles of the beam reaches a maximum RMS value when the beam has traveled through a phase advance of $n\mu = \pi$ before it eventually returns to its initial polarization. To confirm our findings, we performed a simple Monte Carlo simulation using a FODO cell with the parameters $\beta_0 = 5$ meters, $\alpha = 1$, $\epsilon_{rms} = 10\pi$ mm·mrad, and a phase advance per cell of $\psi = 0.283541$ radians, since irrational numbers make it easier to illustrate the effects. The results of the simulation are illustrated in Figure 4.14.

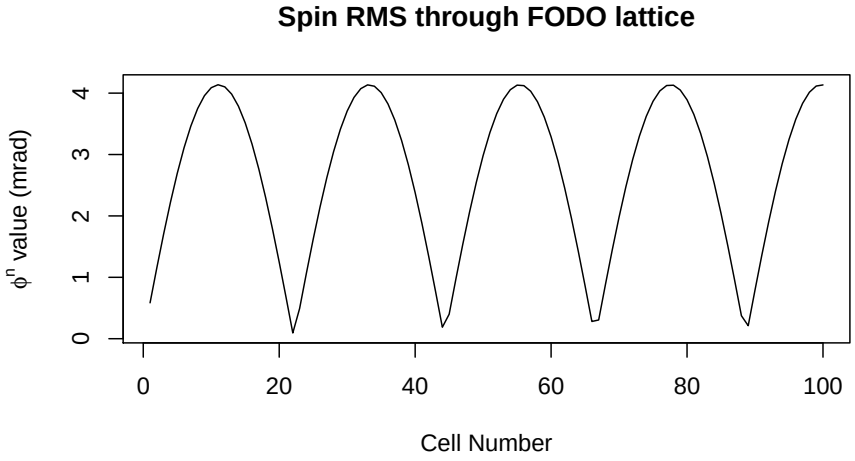

Figure 4.14: As we can see above, a perfectly polarized beam passes through a FODO lattice and reaches a peak value after a number of cells before returning toward its original configuration of pure polarization.

4.5.2 Misalignment Effects on Polarization

In chapter 2, we looked at the ideal lattice, but we can expand our model to include cases where a magnet may be misaligned. Looking at figure 4.15, we can see that an ideal particle will be "kicked" by the field of a misaligned magnet. This will result in a betatron oscillation through the remaining lattice.

Mathematically, we can describe the effects of the misalignment using our Courant-Snyder matrix, only adding a term at the end to the slope (due to the change in the field gradient due to the misalignment). Because the trajectory itself is continuous, the x term is unchanged. Thus, we can write

$$\begin{pmatrix} x \\ x' \end{pmatrix} = \begin{pmatrix} a & b \\ c & d \end{pmatrix} \begin{pmatrix} x_0 \\ x'_0 \end{pmatrix} + \begin{pmatrix} 0 \\ \Gamma \end{pmatrix} \tag{4.35}$$

Now, the value for Γ is dependent on the strength of the magnet, as well as the amount of the displacement. Since the value for Γ simply represents a change in slope value x' due to

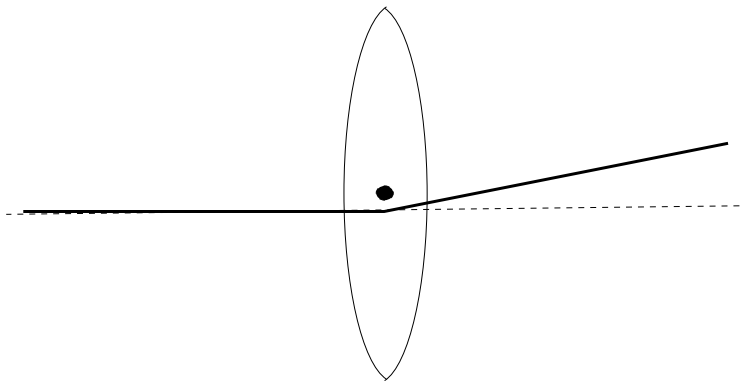

Figure 4.15: A particle traveling along the ideal trajectory will be bent by a misaligned magnet.

the misalignment, and we can clearly see that a magnet misaligned by a value of d would change the slope by a factor of

$$\Delta x' = \frac{d}{F} \equiv \Gamma \tag{4.36}$$

where F is the focal length of the quadrupole. A key takeaway from this equation is that misalignment is a *linear* effect. So when analyzing the effects of the misalignments on a beam lattice, we can simply sum the effects of each magnet.

For a single magnet with misalignment of d, we can write

$$\Delta x_{end} = \frac{d}{F}\sqrt{\beta_1 \beta_2}\sin\psi_{1\to 2} \tag{4.37}$$

Where the particle encounters a misaligned magnet at a lattice location 1 with β_1 and phase ψ_1 and we want to know it's ultimate displacement at point 2, with β_2 and phase ψ_2. For a series of misalignments, and a final beta value of β_f we could sum these values and get

$$\Delta x_{end} = \sum_{i=1}^{N} \frac{d_i}{F_i}\sqrt{\beta_i \beta_f}\sin\psi_{i\to 2} \tag{4.38}$$

Squaring both sides and taking averages yields

$$< \Delta x^2 >=< d^2 > \beta_f \left\langle \frac{\beta}{F^2} \right\rangle \frac{N}{2} \tag{4.39}$$

Now, taking the square root of both sides to get the RMS value gives our result for the RMS position

$$\Delta x_{rms} = d_{rms} \sqrt{\beta_f \left\langle \frac{\beta}{F^2} \right\rangle} \sqrt{\frac{N}{2}} \tag{4.40}$$

We ultimately want to look at the change in the slopes, $\Delta x'$. For an ideal particle, the misaligned magnet will change the slope to d/F at some point along the beamline. This allows us to use our Courant-Snyder matrix with starting values $(x, x') = (0, d_i/F_i)$ to write

$$\Delta x' = \sum_{i=1}^{N} \frac{d_i}{F_i} (\cos\psi - \alpha_f \sin\psi) \sqrt{\frac{\beta_i}{\beta_f}} \tag{4.41}$$

We follow the pattern of squaring both sides, averaging over all the particles in a distribution and then taking the square root to get

$$\Delta x'_{rms} = d_{rms} \sqrt{\left\langle \frac{\beta}{F^2} \right\rangle \frac{1}{\beta_f} \left(\frac{1}{2} + \frac{\alpha_f^2}{2} \right)} \sqrt{N} \tag{4.42}$$

We can utilize the definition of the Courant-Snyder parameter γ, $\gamma = \frac{1+\alpha^2}{\beta}$ and write our answer as

$$\Delta x'_{rms} = d_{rms} \sqrt{\gamma_f \left\langle \frac{\beta}{F^2} \right\rangle} \sqrt{\frac{N}{2}} \tag{4.43}$$

Plugging this into equation 4.4, we would have

$$\Delta \phi_{rms} = (1 + a\gamma_r) d_{rms} \sqrt{\gamma_f \left\langle \frac{\beta}{F^2} \right\rangle} \sqrt{\frac{N}{2}} \tag{4.44}$$

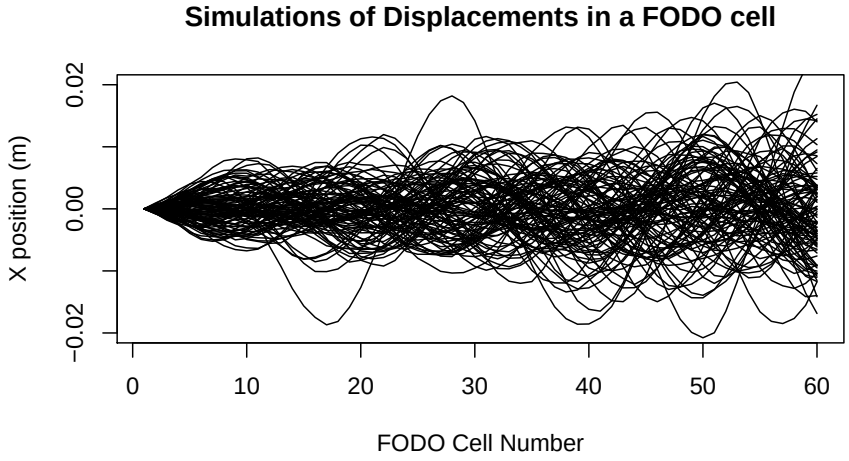

Figure 4.16: The trajectories of a particle through an idealized FODO cell with random misalignments.

It's important to see how this ties into our expectation. We know from Chapter 2 that our x values are proportional to the Courant-Snyder β, and the x' values are proportional to the Courant-Snyder γ, so it serves as a good confirmation that the effects of misaligments give $\Delta x_{rms} \propto \beta$ and $\Delta x'_{rms} \propto \gamma$.

For a brief moment, we'll take a look at the results of simulations on a FODO lattice, where, for simplicity, we picked a lattice consisting of 60 repeating cells with $\beta = 5$ m and $\psi = 0.287541$ radians, since an irrational phase better illustrates the effect. The results of a few tracks with random displacements are shown in figure 4.16. It's easy to see that the misalignments create a range of possible bounded trajectories and slopes, based on the scale of the displacements (in this case, we used a random displacement with 0.250 mm). Returning to the beamline required for g-2, if we were to plug in $a \approx 0.001$, $\gamma \approx 30$ and the known values for the M2M3 beamline ($\beta = 5.0328$ m & $\alpha = -0.72738$), and using an RMS displacement of 0.250 mm, and the M2M3 values for $\frac{\beta}{F^2} = 1.3$ m^{-1} for 60 quadrupoles (along with our previous values for $a \approx 0.001$ and $\gamma \approx 30$) gives a $\Delta\phi_{rms} \approx 1$ mrad.

4.5.3 Momentum Spread Effects on Polarization

Up to this point, we've assumed that all particles traveling along the beamline have the same momentum, but that is rarely the case. We can take a moment to think about the effects of particles with various momenta passing through a bending magnet. From the Thomas-BMT equation (3.4) the excess spin precession in the plane perpendicular to the magnetic field and relative to the particle trajectory is

$$\Delta\phi = a\gamma\theta \tag{4.45}$$

So the spread in $\Delta\phi$ due to a spread in momentum can be written as

$$d\Delta\phi = a\gamma\theta\frac{d\gamma}{\gamma} \tag{4.46}$$

Taking the RMS of both sides gives

$$\Delta\phi_{rms} = a\gamma\theta\left(\frac{d\gamma}{\gamma}\right)_{rms} \tag{4.47}$$

For a highly relativistic beam, the term $\frac{d\gamma}{\gamma}$ is our momentum spread, so we can approximate the effects on the beam polarization using values of $a \approx 0.001$, $\gamma \approx 30$, and $\frac{dp}{p} = 1.5\%$. Using a θ of 0.2 rad (10°), which is appropriate for the M2M3 beamline, we get a spread of about $\Delta\phi_{rms} \approx 0.1$ mrad. For the Delivery Ring, we have an angle of 4 turns of 2π radians which gives a spin spread of $\Delta\phi_{rms} \approx 11$ mrad.

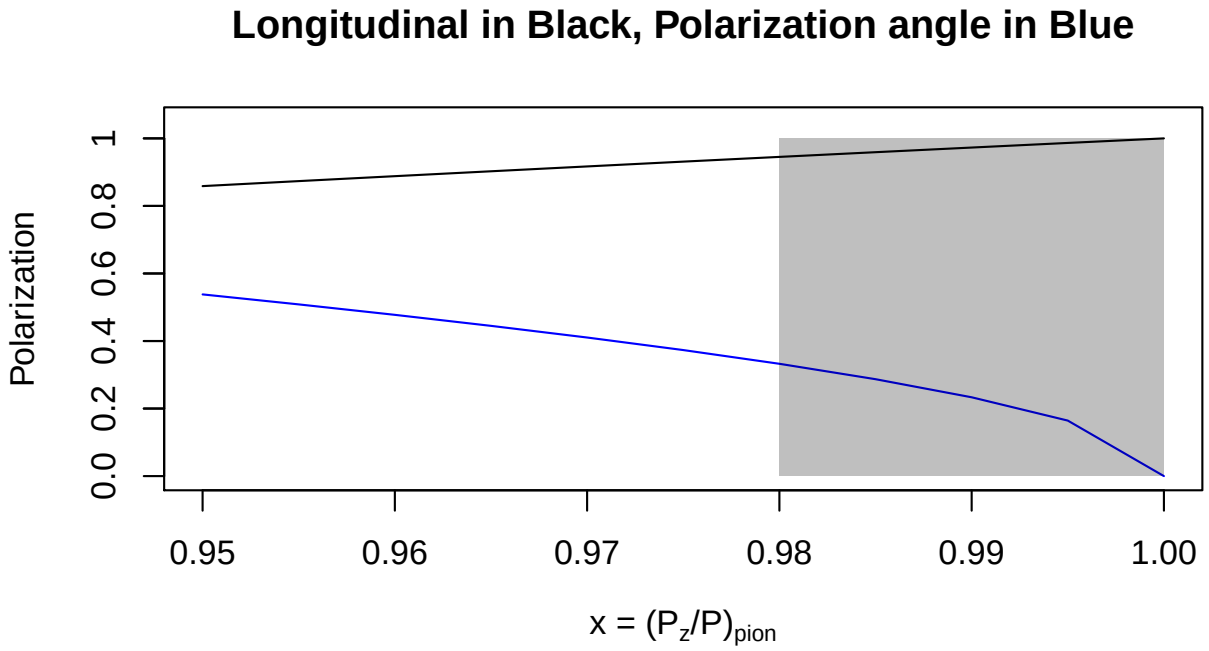

Figure 4.17: The polarization of the beam based on the momentum ratios of the pions.

4.5.4 Particle Decay Effects on Polarization

The muon beam is created by decaying pions, and from the work of Combley and Picasso [23], a relationship exists between the longitudinal polarization Σ_L and the momentum ratio $x = p_{\parallel}/p$ based on the equation

$$\Sigma_L = \cos\phi = \frac{x(1+b^2) - 2b^2}{x(1-b^2)} \tag{4.48}$$

We can plot this and see that we would expect spin spread on the order of 300 ($\pm$100) mrad. Figure 4.17 shows the values for ϕ, the polarization angle (in radians), and Σ_L, the longitudinal beam polarization, versus x. The parameter b is the ratio of masses

$$b = \frac{m_\mu}{m_\pi} = 0.757 \tag{4.49}$$

The blue line denotes the polarization angle, ϕ (in radians), and the black line denotes the longitudinal polarization Σ_L. We can see that a beam which has a longitudinal polarization of 98 % would still see a spread in spin angles of hundreds of mrad (denoted by the shaded region in the graph). This is consistent with the results from our G4beamline simulations which include pion decays.

4.5.5 Interpreting spread results

We want to show that the spin orientations we're dealing with, while they are interpreted in three dimensions, the angles in the x and y directions are small enough that we can treat them as independent of each other. To do this, we'll begin with our rotation matrices, and show that for $\theta << 1$, the product of two rotations are commutative, that is $R_x \cdot R_y = R_y \cdot R_x$. We first begin by computing both matrices

$$\begin{pmatrix} 1 & 0 & 0 \\ 0 & \cos(\theta) & -\sin(\theta) \\ 0 & \sin(\theta) & \cos(\theta) \end{pmatrix} \cdot \begin{pmatrix} \cos(\theta) & 0 & \sin(\theta) \\ 0 & 1 & 0 \\ -\sin(\theta) & 0 & \cos(\theta) \end{pmatrix} = \begin{pmatrix} \cos(\theta) & 0 & \sin(\theta) \\ \sin^2(\theta) & \cos(\theta) & -\sin(\theta)\cos(\theta) \\ -\sin(\theta)\cos(\theta) & \sin(\theta) & \cos^2(\theta) \end{pmatrix} \tag{4.50}$$

With the opposite rotation order $(R_y \cdot R_x)$ giving the result

$$\begin{pmatrix} \cos(\theta) & 0 & \sin(\theta) \\ 0 & 1 & 0 \\ -\sin(\theta) & 0 & \cos(\theta) \end{pmatrix} \cdot \begin{pmatrix} 1 & 0 & 0 \\ 0 & \cos(\theta) & -\sin(\theta) \\ 0 & \sin(\theta) & \cos(\theta) \end{pmatrix} = \begin{pmatrix} \cos(\theta) & \sin^2(\theta) & \sin(\theta)\cos(\theta) \\ 0 & \cos(\theta) & -\sin(\theta) \\ -\sin(\theta) & \sin(\theta)\cos(\theta) & \cos^2(\theta) \end{pmatrix} \tag{4.51}$$

It's clear to see that the diagonal elements are all equal, so we're left to show that the off-diagonal elements are equal when we take small angles into account. Using $\sin(\theta) \approx \theta$ and $\cos(\theta) \approx 1 - \frac{\theta^2}{2}$, we just need to show the following identities hold for small values of θ.

$$\pm \sin(\theta)\cos(\theta) = \pm \sin(\theta) \tag{4.52}$$

$$\sin^2(\theta) \approx 0 \tag{4.53}$$

For our first equation, we have

$$\pm \sin(\theta)\cos(\theta) \approx \pm\theta(1 - \frac{\theta^2}{2}) \tag{4.54}$$

$$\approx \pm\theta \mp \frac{\theta^3}{2} \tag{4.55}$$

We know from above that our spin angles have orders of magnitude somewhere around 10^{-3}, so the second term is $(10^{-3})^2 \approx 0$, so we have

$$\pm \sin(\theta)\cos(\theta) \approx \pm\theta \approx \pm \sin(\theta) \tag{4.56}$$

Using a similar argument, we know that $(10^{-3})^3 \approx 0$, so we have

$$\sin^2(\theta) \approx \theta^2 \approx 0 \tag{4.57}$$

Table 4.1: The table illustrates the magnitude of the effects on the RMS of the spin spread due to the individual factors.

Source	ϕ_{RMS}
Emittance	≈ 2.7 mrad
Misalignments	≈ 1 mrad
Momentum spread	≈ 11 mrad
Particle decays	≈ 300 (± 100) mrad

Using these two substitutions allows us to see that equations 4.50 and 4.51 are equivalent for small angles. The commutative relationship at small angles allows us to investigate our spin angles independently of one another in our analytical estimates. Of course, in the numerical simulations we did not make any of these approximations.

4.6 Conclusions

The purpose of this study was to understand how the spin dynamics of a particle beam evolve throughout a beamline and how the phase space parameters influence beam polarization as a whole. It utilized the Muon g-2 experiment as a test case and provided necessary analysis of the delivery system.

With respect to the g-2 experiment, we see that efforts to ensure alignment accuracy better than 250 μm are important for efficient particle transport, but ultimately do not improve beam polarization. While factors such as emittance, misalignments, and momentum spread could conceivably contribute to the measurement of MDM and search for a non-zero EDM in the Muon g-2 experiment, we've discovered that the beam polarization generated by pion decay dominates these other effects as evidenced by the results of Table 4.1.

Looking at particle beam spin dynamics as a whole, understanding the contributions of the phase space variables to the beam polarization helps to build a foundation upon which future analyses will be based. Two important correlations were identified. The momentum spread creates a correlation between the momentum of the particles and their spin direction, since lower momentum particles experience a greater spin precession than higher momentum particles. The emittance of the beam also produces a correlation between the betatron oscillation amplitude and the spin, where particles further from the ideal path precess more than those which are closer, due to the higher strength of the fields encountered in focusing quadrupoles. Expanding the understanding of these relationships will be important as we turn our attention to future work in which improved methods of EDM measurements for particles such as protons, which do not depend on decays for creation, will be examined.

REFERENCES

[1] J. Grange et al. . Muon (g-2) technical design report (DocDB 2055), 2015. Available from: http://gm2-docdb.fnal.gov:8080/cgi-bin/RetrieveFile?docid=2055&filename=TDR-E989-CD3Rev-final3.pdf&version=7

[2] D. A. Edwards & M. J. Syphers. *An introduction to the physics of high energy accelerators*. Wiley VCH, Weinheim, Germany, pp.57-98, 1993.

[3] E. D. Courant & H. S. Snyder. Theory of the alternating gradient synchrotron. *Annals of Physics*, **3**(1), 1-48, 1958.

[4] H. Yukawa. On the interaction of elementary particles. *Proc. Phys. Math. Soc. Japan*, **17**, 48, 1935.

[5] P. Kunze. Untersuchung der ultrastrahlung in der Wilsonkammer. *Zeitschrift für Physik*, **80**(9), 1 Fig 5, 1933.

[6] C. D. Anderson & S. H. Neddermeyer. Cloud chamber observations of cosmic rays at 4300 meters elevation and near sea-level. *Physical Review*, 1936, **50**, 263.

[7] S. H. Neddermeyer, & C. D. Anderson. Note on the nature of cosmic-ray particles. *Physical Review*, **51**, 844, 1937.

[8] J. C. Street, & E. C. Stevenson. New evidence for the existence of a particle of mass intermediate between the proton and electron. *Physical Review*, **52**, 1003, 1937.

[9] Y. Nishina, M. Tekeuchi, & T. Ichimiya. On the nature of cosmic-ray particles. *Physical Review*, **52**, 1198, 1937.

[10] M. M. J. Crussard, & L. Leprince-Ringuet. Études de traversées d'écrans de plomb par des électrons du rayonnenent cosmique de 200 1 000 millions d'élecron-volts et observations de phénomènes divers. *Journal de Physique et le Radium*, **8**(5), 213-216, 1937.

[11] P. A. M. Dirac. The quantum theory of the electron. *Proceedings of the Royal Society of London*, **A117**(778), 610-624, 1928.

[12] J. P. Miller, E. de Rafael, & B. L. Roberts. Muon g-2: Review of theory and experiment. *Reports on Progress in Physics*, **70**(5), 15, 2007.

[13] G. W. Bennett et al. Final report of the muon E821 anomalous magnetic moment measurement at BNL. *Physical Review D*, **73**(7), 90, 2006.

[14] L. H. Thomas. The kinematics of an electron with an axis. *The London, Edinburgh, and Dublin Philosophical Magazine and Journal of Science*, **3**(13), 1-22, 1927.

[15] V. Bargmann, L. Michel, & V. L. Telegdi. Precession of the polarization of particles moving in a homogeneous electromagnetic field. *Physical Review Letters*, **2**(10), 435, 1959.

[16] European Organization for Nuclear Research . MADx (Methodical Accelerator Design) Version 5.02.00. [Computer software], 1990. Accessed from: http://madx.web.cern.ch/madx

[17] T. Roberts. G4beamline Version 3.02.1 [Computer software], 2004. Accessed from: http://g4beamline.muonsinc.com

[18] Python Software Foundation. Python Version 3.5.2 [Computer software], 2001. Accessed from: https://www.python.org/downloads/

[19] R Core Team. R: A language and environment for statistical computing [Computer software]. R Foundation for Statistical Computing, Vienna, Austria, 2013. Accessed from: http://www.R-project.org/

[20] M. Korostelev. Distribution of protons at the exit of the production target (DocDB 4404), 2016. Accessed from: http://gm2-docdb.fnal.gov:8080/cgi-bin/ShowDocument?docid=4404

[21] M. Korostelev, et al. Effects of transverse misalignments of quadrupoles in the transport lines and delivery ring (DocDB 4527), 2016. Accessed from: http://gm2-docdb.fnal.gov:8080/cgi-bin/ShowDocument?docid=4527

[22] D. Sagan. Bmad [Computer software], (n.d.). Accessed from: https://www.classe.cornell.edu/ dcs/bmad/overview.html

[23] F. Combley & E. Picasso. The muon (g-2) precession experiments: Past, present and future. *Physics Reports*, **14**(1), 20, 1974.

APPENDIX

MATHEMATICAL FORMULATION FOR BEAM PHYSICS

The purpose of this appendix is to provide a more rigorous derivation of the results in Chapter 2.

The following derivation follows Edwards & Syphers ([2], pp. 60-65).
We should note that our quadrupole magnet is designed such that there is no free current ($J = 0$) and no electric field ($\vec{E} = 0$), which reduced equation 2.5 to

$$\nabla \times \vec{B} = 0 \tag{A.1}$$

Taking our curl of $\vec{B}$ gives us the following result.

$$\nabla \times \vec{B} = \Big(\frac{\partial B_s}{\partial y} - \frac{\partial B_y}{\partial s}\Big)\hat{x} + \Big(\frac{\partial B_x}{\partial s} - \frac{\partial B_s}{\partial x}\Big)\hat{y} + \Big(\frac{\partial B_y}{\partial x} - \frac{\partial B_x}{\partial y}\Big)\hat{s} \tag{A.2}$$

The result from equation A.1 means that all components must identically vanish to 0 simultaneously. The design of the magnet is such that inside the magnet there are no fields in the $\hat{s}$ direction (while fringe fields do occur on the edges of the magnet, we're ignoring them at the moment), which implies $B_s = 0$, this leaves us with only the $\hat{s}$ component where non-zero values could occur.

$$\Big(\frac{\partial B_y}{\partial x} - \frac{\partial B_x}{\partial y}\Big) = 0 \tag{A.3}$$

Taylor expansion of the B_x and B_y fields gives our results for small deviations

$$B_x = B_x(0,0) + \frac{\partial B_x}{\partial x} \cdot x + \frac{\partial B_x}{\partial y} \cdot y + ... \tag{A.4}$$

$$B_y = B_y(0,0) + \frac{\partial B_y}{\partial y} \cdot y + \frac{\partial B_y}{\partial x} \cdot x + ... \tag{A.5}$$

For particles traveling close to c, we can treat our magnet as a thin element

$$B_y = \frac{\partial By}{\partial x} \cdot x = B' \cdot x \tag{A.6}$$

This gives us two equations.

$$x_f = x_i \tag{A.7}$$

$$x'_f = x'_i - \frac{l}{\rho} \tag{A.8}$$

Diverge for a moment to think of particle in uniform B field.

$$\frac{\gamma m v^2}{\rho} = qv \times B \tag{A.9}$$

Rearranging terms, and noting that γmv is the relativistic momentum gives us the following identity

$$(B\rho) = \frac{p}{q} \tag{A.10}$$

The value $(B\rho)$ is referred to as the magnetic rigidity. This will allow us to re-write equation A.8 as

$$x'_f - x'_i = -\frac{l}{\rho} = -\frac{le}{p} B_y \tag{A.11}$$

$$\Delta x' = -\frac{le}{p} B' x \tag{A.12}$$

Now, we just have one final piece of the puzzle to complete our process. We can imagine our magnet as a lens, and picture the trajectory of a particle entering the lens with an initial value of $x' = 0$. This is illustrated in A.1. Since the focal length, f, is much larger than the deviation from the ideal path, x, we can treat the angle through which a particle is bent using a small angle approximation, $\tan(\theta) \approx \theta$. This means we can say our angle is simply $\Delta x'$, and we get

$$\Delta x' = -\frac{x}{f} \tag{A.13}$$

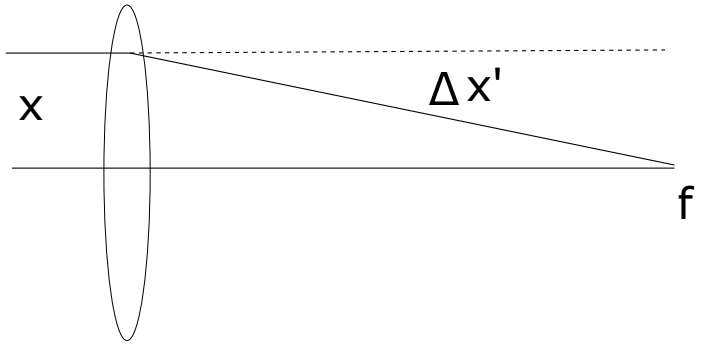

Figure A.1: A particle entering above the centerline of the focusing lens with an initial value of $x' = 0$ is bent toward the focal point.

So our $\Delta x'$ value is now related to both the x position, and a focal length. Substituting all of this back into equation A.12 gives us the following identity.

$$\frac{1}{f} = \frac{eB'l}{p} \tag{A.14}$$

It also allows us to rewrite equation A.8 as

$$x'_f = x'_i - \frac{x}{f} \tag{A.15}$$

This is for the case of a thin focusing magnet. If the magnet were defocusing, we would simply change the sign on the last term.

A.1 A Case Study: The FODO Cell

For a simple example, we can look at a particle that travels through a focusing magnet with focal length F, followed by a drift space of length L, a defocusing magnet with focal length F, and a final drift space of length L. A repetitive arrangement of this kind is known as a FODO lattice (with F and D representing Focusing and Defocusing, and O representing

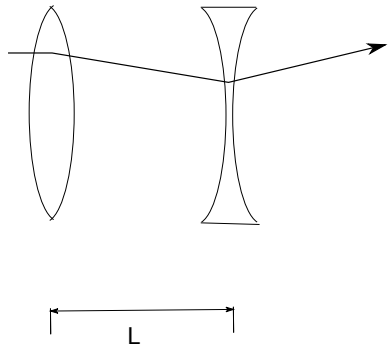

Figure A.2: A FODO cell which has an example particle trajectory denoted by the thick line with arrow.

a drift space). A visual of this particular arrangement is in figure A.2. While visualizations are good, we ultimately need to be able to describe the motion of the particle. We can use our thin lens equations (A.7 and A.12), but we also need to add two equations, which describe the motion of the particle in a drift space.

$$x_f = x_i + vt \tag{A.16}$$

Unfortunately, we don't have the time or velocity values readily available. Let's instead try to rewrite these equations in terms of known values, using our definitions of velocity.

$$x_f = x_i + \frac{dx}{dt}t = x_i + \frac{dx}{ds}\frac{ds}{dt}t \tag{A.17}$$

But we know that $\frac{dx}{ds} = x'$, and the term $t\frac{ds}{dt}$ simply reduces to the length of s, which in this case is L. Finally, we have our equations for a drift space.

$$x_f = x_i + Lx_i' \tag{A.18}$$

$$x_f' = x_i' \tag{A.19}$$

Since there is no force to change the trajectory of the particle, the slope is simply constant. In looking at our equations above, we can actually use a matrix notation to represent our equations for a drift space.

$$\begin{pmatrix} x_f \\ x'_f \end{pmatrix} = \begin{pmatrix} 1 & L \\ 0 & 1 \end{pmatrix} \begin{pmatrix} x_i \\ x'_i \end{pmatrix} \tag{A.20}$$

Additionally, using equations A.7 and A.12 we can create the matrix for a focusing quadrupole magnet.

$$\text{Focusing} \quad \text{Matrix} = \begin{pmatrix} 1 & 0 \\ -\frac{1}{f} & 1 \end{pmatrix}$$

With the only noticeable difference between the focusing and defocusing lens that the defocusing lens has a positive sign in the lower left element.

A.1.1 Matrix Representation

By multiplying matrices together, we could represent an entire beamline using only a single matrix created from all the beamline elements. For a FODO lattice, we have

$$M = \begin{pmatrix} 1 & L \\ 0 & 1 \end{pmatrix} \begin{pmatrix} 1 & 0 \\ \frac{1}{F} & 1 \end{pmatrix} \begin{pmatrix} 1 & L \\ 0 & 1 \end{pmatrix} \begin{pmatrix} 1 & 0 \\ -\frac{1}{F} & 1 \end{pmatrix} = \begin{pmatrix} 1 - \frac{L}{F} - \left(\frac{L}{F}\right)^2 & 2L + \frac{L^2}{F} \\ -\frac{L}{F^2} & 1 + \frac{L}{F} \end{pmatrix} \tag{A.21}$$

The lattice remains stable ([2], pp. 64-65) when

$$-2 \leq \mathrm{Tr}M \leq 2 \tag{A.22}$$

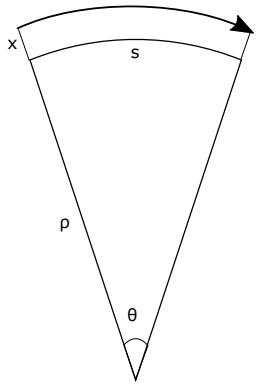

Figure A.3: The figure illustrates a particle traveling at a displaced value x from the ideal radius ρ.

For our FODO cell, it looks like

$$|\frac{L}{2F}| \leq 1 \tag{A.23}$$

A.2 Transverse equations of motion

This section follows ([2] pp. 66-74)

Our first task is to define some relations which will become useful later on, and to start with the equations in the x direction. We want to describe the motion of a particle using figure A.3. So we first start with our geometric relation, $\Delta s = \Delta\theta\rho$. But we need a way to relate our unit vectors as well. We remember that $\hat{r}$ is along the path of motion, and $\hat{x}$ is perpendicular to $\hat{s}$ along the radius. This gives the relation

$$\Delta\hat{x} = \Delta\theta\hat{s} \tag{A.24}$$

Which has a derivative form

$$\dot{\hat{x}} = \dot{\theta}\hat{s} \tag{A.25}$$

Since we ultimately need a time derivative for $\hat{s}$, we can note that

$$\dot{\hat{s}} = -\dot{\theta}\hat{x} \tag{A.26}$$

We also need to note that the radius of travel for our particle is defined by

$$r = \rho + x \tag{A.27}$$

And utilizing kinematics, we can say that the time a particle takes to travel on path s is related to the velocity of a particle in the $\hat{s}$ direction and the time of the travel. $\Delta s = v\Delta t$. But we already know from geometry that $\Delta s = \Delta\theta\rho$, so we can equate these two values to get

$$v\Delta t = r\Delta\theta \tag{A.28}$$

$$v_s = r\dot{\theta} \tag{A.29}$$

$$\dot{\theta} = \frac{v_s}{r} \tag{A.30}$$

Having completed these relations, we can now begin our derivation.

$$\frac{d\vec{p}}{dt} = q\vec{v} \times \vec{B} \tag{A.31}$$

We first perform the cross product on the right hand side and get

$$\vec{v} \times \vec{B} = \det \begin{bmatrix} \hat{x} & \hat{y} & \hat{s} \\ v_x & v_y & v_s \\ B_x & B_y & B_s \end{bmatrix}$$

This gives us a determinant of

$$(v_y B_s - v_s B_y)\hat{x} + (v_s B_x - v_x B_s)\hat{y} + (v_x B_y - v_y B_x)\hat{s} \tag{A.32}$$

Since our field's orientation is such that there are no magnetic fields in the $\hat{s}$ direction, so $B_s = 0$ This leaves us with

$$(-v_s B_y)\hat{x} + (v_s B_x)\hat{y} + (v_x B_y - v_y B_x)\hat{s} \tag{A.33}$$

We're neglecting the last term as second order in our variables in x and x'. We can now rewrite the left hand side of equation A.31 as

$$\frac{d\vec{p}}{dt} = \frac{d\gamma m\vec{v}}{dt} = \frac{\gamma m d\vec{v}}{dt} \tag{A.34}$$

Now, we can come up with a general equation describing the position of a particle in the transverse plane.

$$\vec{R} = r\hat{x} + y\hat{y} \tag{A.35}$$

We will now take derivatives with respect to time to get

$$\vec{R} = (\rho + x)\hat{x} + y\hat{y} \tag{A.36}$$

$$\dot{\vec{R}} = \dot{r}\hat{x} + r\dot{\hat{x}} + \dot{y}\hat{y} \tag{A.37}$$

We then substitute using equation A.25 to rewrite A.37 as

$$\dot{\vec{R}} = \dot{r}\hat{x} + \theta r\dot{\hat{s}} + \dot{y}\hat{y} \tag{A.38}$$

We will now take our second derivative with respect to time

$$\ddot{\vec{R}} = \ddot{r}\hat{x} + \dot{r}\dot{\hat{x}} + \ddot{\theta}r\hat{s} + \dot{\theta}r\dot{\hat{s}} + \ddot{y}\hat{y} \tag{A.39}$$

We'll utilize equation A.25 again and combine terms to get

$$\ddot{\vec{R}} = (\ddot{r} - r\dot{\theta}^2)\hat{x} + \ddot{y}\hat{y} + (2\dot{r}\ddot{\theta} + r\theta)\hat{s} \tag{A.40}$$

It's important to note that the first term is $\ddot{\vec{R}}_x$ and the second term is $\ddot{\vec{R}}_y$. We'll first examine $\ddot{\vec{R}}_x$ by plugging our position into equation A.34.

$$\frac{\gamma m d\vec{v}}{dt} = \gamma m\dot{\vec{v}} \tag{A.41}$$

$$= \gamma m\ddot{\vec{R}} \tag{A.42}$$

$$= \gamma m[(\ddot{r} - r\dot{\theta}^2)\hat{x} + \ddot{y}\hat{y} + (2\dot{r}\ddot{\theta} + r\theta)\hat{s}] \tag{A.43}$$

And our result is

$$\gamma m[(\ddot{r} - r\dot{\theta}^2)\hat{x} + \ddot{y}\hat{y} + (2\dot{r}\ddot{\theta} + r\theta)\hat{s}] = q[(-v_s B_y)\hat{x} + (v_s B_x)\hat{y} + (v_x B_y - v_y B_x)\hat{s}] \tag{A.44}$$

Start with the $\hat{x}$ component.

$$\gamma m(\ddot{r} - r\dot{\theta}^2) = (-qv_s B_y) \tag{A.45}$$

If we were to divide both sides by γm and multiply the right hand side by $\frac{v_s}{v_s}$ we would have

$$\ddot{r} - r\dot{\theta}^2 = -\frac{qv_s^2 B_y}{\gamma m v_s} = -\frac{q}{p}v_s^2 B_y \tag{A.46}$$

We use our magnetic rigidity equation (A.10) and get

$$\ddot{r} - r\dot{\theta}^2 = -\frac{v_s^2 B_y}{B\rho} \tag{A.47}$$

Remove the time derivatives and instead rewrite them as spatial derivatives with respect to the variable s.

$$\frac{d}{dt} = \frac{ds}{dt}\frac{d}{ds} \tag{A.48}$$

Geometrically, we know that $ds = \rho d\theta$, and

$$r\frac{d\theta}{dt} = v_s \tag{A.49}$$

We combine to get

$$\frac{ds}{dt} = \frac{\rho v_s}{r} \tag{A.50}$$

Our second derivative can be written as

$$\frac{d^2}{dt^2} = \left(\frac{ds}{dt}\right)^2 \left(\frac{d^2}{ds^2}\right) = \left(\frac{\rho v_s}{r}\right)^2 \left(\frac{d^2}{ds^2}\right) \tag{A.51}$$

So, we now write (substituting $r = \rho + x$)

$$\ddot{r} = \frac{d^2 r}{dt^2} = \left(\frac{v_s p}{r}\right)^2 \left(\frac{d^2 r}{ds^2}\right) = \left(\frac{v_s \rho}{\rho + x}\right)^2 \left(\frac{d^2(\rho + x)}{ds^2}\right) \tag{A.52}$$

Since ρ is just a constant, we know that

$$\frac{d^2(\rho + x)}{ds^2} = \frac{d^2(x)}{ds^2} = x'' \tag{A.53}$$

We now can rearrange our value for the second time derivative of r, using a Taylor approximation and ignoring terms of second order or higher in x and x''

$$\ddot{r} = \frac{v_s^2 \rho^2}{(\rho + x)^2}(x'') \tag{A.54}$$

$$= \frac{v_s^2 \rho^2}{\rho^2 \left(1 + \frac{x}{\rho}\right)^2} x'' \tag{A.55}$$

$$= v_s^2 \left(1 - 2\frac{x}{\rho}\right) x'' \tag{A.56}$$

$$\approx v_s^2 x'' \tag{A.57}$$

Substituting our result into our equation of motion (A.47), along with the identity $\dot{\theta} = v_s/r$ to get

$$v_s^2 x'' - (\rho + x)\left(\frac{v_s}{(\rho + x)}\right)^2 = -\frac{v_s^2 B_y}{B\rho} \tag{A.58}$$

We can certainly cancel some terms (v_s) and factor to get

$$x'' - \frac{1}{(\rho + x)} = -\frac{B_y}{B\rho} \tag{A.59}$$

$$x'' - \frac{1}{\rho}\left(1 - \frac{x}{\rho}\right) = -\frac{B_y}{B\rho} \tag{A.60}$$

Now we need an expression for B_y, which we can approximate via Taylor expansion, ignoring higher order terms since we're only concerned with small oscillations.

$$B_y = B_y(0,0) + \frac{\partial B_y}{\partial y} y + \frac{\partial B_y}{\partial x} x + ... \tag{A.61}$$

Because we're capable of designing our accelerator to have uncoupled motion, $\frac{\partial B_y}{\partial y} = 0$. But we also know that the fields change along the beam trajectory, so we have $B_y(s)$, that is, the magnetic field is a function of position. We now write our equation of motion

$$x'' - \frac{1}{\rho}\left(1 - \frac{x}{\rho}\right) = \frac{1}{B\rho}\left(B_y(0,0) + \frac{\partial B_y(s)}{\partial x}x\right) \tag{A.62}$$

We can rewrite our equation as

$$x'' - \frac{1}{\rho} + \frac{x}{\rho^2} = -\frac{1}{B\rho}\left(B_y(0,0) + \frac{\partial B_y(s)}{\partial x}x\right) = -\left(\frac{1}{\rho} + \frac{\partial By/\partial x}{B\rho}\cdot x\right) \tag{A.63}$$

Rearranging and combining terms gives

$$x'' + \left(\frac{1}{\rho^2} + \frac{1}{B\rho}\frac{\partial B_y(s)}{\partial x}\right)x = 0 \tag{A.64}$$

This equation is similar to a harmonic oscillator, with the term $\frac{1}{\rho^2}$ corresponding to dipole focusing and $\frac{1}{B\rho}\frac{\partial B_y(s)}{\partial x}$ corresponding to the quadrupole focusing term. A future task is to find a solution to equation A.64.

Now, let us examine the motion in the $\hat{y}$ direction. Equating the y components of equation A.44

$$\gamma m\ddot{y} = qv_sB_x \tag{A.65}$$

Similarly as we did for x, we can divide by γm and multiply the right hand side by $\frac{v_s}{v_s}$ to get

$$\ddot{y} = \frac{qv_s^2B_x}{\gamma mv_s} \tag{A.66}$$

Noting that $\gamma m v_s = p$, and using our rigidity condition, we have

$$\ddot{y} = \frac{v_s^2 B_x}{(B\rho)} \tag{A.67}$$

Once more utilizing a change of independent variables from t to s via equation A.48 gives

$$\ddot{y} = \left(\frac{v_s \rho}{r}\right)^2 y'' \tag{A.68}$$

Using this result to replace the left hand side of equation A.67 to get

$$\left(\frac{v_s \rho}{r}\right)^2 y'' = \frac{v_s^2 B_x}{(B\rho)} \tag{A.69}$$

Cancelling like terms, substituting $r = \rho + x$ and isolating y'' gives

$$y'' = \frac{B_x}{(B\rho)} \left(\frac{1}{\rho^2}\right) (\rho + x)^2 \tag{A.70}$$

We can expand B_x via a Taylor series

$$B_x = B_x(0,0) + \frac{\partial B_x}{\partial x} x + \frac{\partial B_x}{\partial y} y + ... \tag{A.71}$$

Substituting this term back into our equation, noting that B_x is a function of s to get

$$y'' = \frac{1}{(B\rho)} \left[B_x(0,0) + \left(\frac{\partial B_y(s)}{\partial x}\right) y \right] \left(1 + \frac{x}{\rho}\right)^2 \tag{A.72}$$

Which reduces to (using the same polynomial expansion on $(1 + \frac{x}{\rho})^2$ and keeping only first order terms)

$$y'' - \frac{1}{(B\rho)} \frac{\partial B_y(s)}{\partial x} y = 0 \tag{A.73}$$

Noting that $\frac{\partial B_x}{\partial y} = \frac{\partial B_y}{\partial x}$ and $B_x(0,0) = 0$ by design (result from the curl condition that $v \times B = 0$ in equation A.3).

A.2.1 Finding a solution

We'll once more focus on the equation of x and then fill in the gaps for y later.
Let us make a small substitution

$$\left(\frac{1}{\rho^2} + \frac{1}{B\rho}\frac{\partial B_y(s)}{\partial x}\right) = K(s) \tag{A.74}$$

We are now able to write our equation as

$$x'' + K(s)x = 0 \tag{A.75}$$

We utilize the need for accelerators to have periodic solutions

$$K(s+c) = K(s) \tag{A.76}$$

We guess that the solution to Hill's equation has a coefficient, A, a variable amplitude scaling term (based on the position, s), and a component to describe the oscillatory behavior, $\cos(\psi(s) + \delta)$. Thus, we have a trial solution

$$x = Aw(s)\cos(\psi(s) + \delta) \tag{A.77}$$

With this trial solution, we can quickly calculate our derivatives.

$$x' = Aw'(s)\cos(\psi(s) + \delta) - Aw(s)\psi'(s)\sin(\psi(s) + \delta) \tag{A.78}$$

Our second derivative is

$$x'' = Aw''(s)\cos(\psi(s)+\delta) + 2Aw'(s)\psi'(s)\sin(\psi(s)+\delta) + Aw(s)\psi''(s)\sin(\psi(s)+\delta) + Aw(s)\psi'^2(s)\sin(\psi(s)+\delta) \quad \text{(A.79)}$$

At this point, the arguments for the w and ψ functions become quite cumbersome, so we'll omit writing them (they're still implied functions of s). Combining like terms, we have

$$x'' + Kx = A(wK + w'' - w\psi'^2)\cos(\psi(s)+\delta) + A(2w'\psi' + w\psi'')\sin(\psi(s)+\delta) \quad \text{(A.80)}$$

Our next step is to note that our trial solution should not depend on the value of δ, and there is no value θ for which $\sin(\theta) = \cos(\theta) = 0$. So that forces our coefficients to both equal 0 simultaneously.

$$wK + w'' - w\psi'^2 = 0 \quad \text{(A.81)}$$

$$2w'\psi' + w\psi'' = 0 \quad \text{(A.82)}$$

The second equation looks promising. If we were to multiply by w it would take the form

$$2ww'\psi' + w^2\psi'' = 0 \quad \text{(A.83)}$$

This then matches the form of the derivative of a product of w^2 and ψ', so we have

$$\frac{d}{ds}w^2\psi' = 0 \quad \text{(A.84)}$$

Integrating both sides implies

$$w^2\psi' = \text{constant} \quad \text{(A.85)}$$

We can call this constant, k, and solve for ψ' in order to substitute it back into the other equation.

$$wK + w'' - w\left(\frac{k}{w^2}\right)^2 = 0 \tag{A.86}$$

$$w^3(w'' + Kw) = k^2 \tag{A.87}$$

We will now solve for the initial conditions of x using our results and the fact that δ is a fixed value.

$$x = Aw(s)\cos(\psi + \delta) \tag{A.88}$$

$$= Aw(s)(\cos(\psi)\cos(\delta) - \sin(\psi)\sin(\delta)) \tag{A.89}$$

$$= A_1\cos(\psi) + A_2\sin(\psi) \tag{A.90}$$

with $A_1 = A\cos(\delta)$ and $A_2 = -A\sin(\delta)$. Doing the same for x' gives

$$x' = Aw'\cos(\psi + \delta) - Aw\psi'\sin(\psi + \delta) \tag{A.91}$$

$$= (A_1w')\cos(\psi) + A_2w'\sin(\psi) - \frac{A_1k}{w}\sin(\psi) + \frac{A_2k}{w}\cos(\psi) \tag{A.92}$$

$$= \left(A_1w' + \frac{A_2k}{w}\right)\cos(\psi) + \left(A_2w' - \frac{A_1k}{w}\right)\sin(\psi) \tag{A.93}$$

Plugging in our initial conditions of (x_i, x_i') at $s = s_i$ gives the result

$$A_1 = \frac{x_0}{w} \tag{A.94}$$

$$A_2 = \frac{x_0'w - x_0w'}{k} \tag{A.95}$$

Once again invoking periodicity and writing our equations in matrix form, we have the result

$$\begin{pmatrix} x \\ x' \end{pmatrix}_{s_0+C} = \begin{pmatrix} \cos(\Delta\psi_C) - \frac{ww'}{k}\sin(\Delta\psi_C) & \frac{w^2}{k}\sin(\Delta\psi_C) \\ -\frac{1+\left(\frac{ww'}{k}\right)^2}{\frac{w^2}{k}}\sin(\Delta\psi_C) & \cos(\Delta\psi_C) + \frac{ww'}{k}\sin(\Delta\psi_C) \end{pmatrix} \begin{pmatrix} x \\ x' \end{pmatrix}_{s_0} \tag{A.96}$$

It should be noted that the term $\Delta\psi_C$ is actually defined as the oscillation (or phase) advance through the repeating lattice. Mathematically, we would write

$$\psi(s_0 \to s_0 + C) \equiv \Delta\psi_C = \int_{s_0}^{s_0+C} \frac{k}{w^2(s)} ds \tag{A.97}$$

Where s_0 is arbitrarily chosen due to the periodicity of the lattice.

A.3 Courant-Snyder Parameters

We define

$$\beta(s) = \frac{w^2(s)}{k} \tag{A.98}$$

$$\alpha(s) = -\frac{1}{2}\left(\frac{d\beta(s)}{ds}\right) = -\frac{1}{2}\frac{d}{ds}\left(\frac{w^2(s)}{k}\right) \tag{A.99}$$

$$\gamma = \frac{1+\alpha^2}{\beta} \tag{A.100}$$

Which allows us to rewrite our matrices as

$$\begin{pmatrix} x \\ x' \end{pmatrix}_{s_0+C} = \begin{pmatrix} \cos(\Delta\psi_C) - \alpha\sin(\Delta\psi_C) & \beta\sin(\Delta\psi_C) \\ -\gamma\sin(\Delta\psi_C) & \cos(\Delta\psi_C) - \alpha\sin(\Delta\psi_C) \end{pmatrix} \begin{pmatrix} x \\ x' \end{pmatrix}_{s_0} \tag{A.101}$$

And our phase advance equation is now

$$\Delta\psi_C = \int_{s_0}^{s_0+C} \frac{1}{\beta(s)} ds \tag{A.102}$$

We can now rewrite our general solution to Hill's equation as

$$x(s) = A\sqrt{\beta(s)}\cos(\psi(s) + \delta) \tag{A.103}$$

Where β is our amplitude function.

If one were to equate the transport matrix in A.101 to an arbitrary 2×2 transport matrix

$$\begin{pmatrix} a & b \\ c & d \end{pmatrix} \tag{A.104}$$

It would be possible to show that we can write a transport matrix from any point (1) to another (2) using the Courant-Snyder parameters at both locations and the phase advance ($\Delta\psi_{1\to 2}$) between them by utilizing the following transport matrix

$$\begin{pmatrix} \left(\frac{\beta_2}{\beta_1}\right)^{1/2}(\cos\Delta\psi + \alpha_1 \sin\Delta\psi) & (\beta_1\beta_2)^{1/2}\sin\Delta\psi \\ -\frac{1+\alpha_1\alpha_2}{(\beta_1\beta_2)^{1/2}} + \frac{1-\alpha_1\alpha_2}{(\beta_1\beta_2)^{1/2}}\cos\Delta\psi & \left(\frac{\beta_1}{\beta_2}\right)^{1/2}(\cos\Delta\psi - \alpha_1\sin\Delta\psi) \end{pmatrix} \tag{A.105}$$

It's important to note that the value for $\Delta\psi$ in the matrix above corresponds to $\psi_2 - \psi_1$.

Returning to the solution to Hill's Equation for a moment, if we take advantage of the identity

$$\alpha(s)x(s) + \beta(s)x'(s) = -A\sqrt{\beta(s)}\sin[\psi(s) + \delta] \tag{A.106}$$

If we square both sides of equations A.106 and A.103, we can sum them to get (noting that the position s is implied for all values)

$$x^2 + \alpha^2 x^2 + 2\alpha\beta x x' + \beta^2 x'^2 = A^2\beta(\cos^2[\psi(s) + \delta] + \sin^2[\psi(s) + \delta]) \tag{A.107}$$

$$\tag{A.108}$$

We can isolate the term A^2 by using the trig identity $\sin^2 x + \cos^2 x = 1$ and dividing both sides by β to get

$$\frac{1 + \alpha^2}{\beta} x^2 + 2\alpha x x' + \beta x'^2 = A^2 \tag{A.109}$$

Using our Courant-Snyder identity, and now including our position variable s, we can write our final answer as

$$A^2 = \gamma(s)x(s)^2 + 2\alpha(s)x(s)x'(s) + \beta(s)x'(s)^2 \tag{A.110}$$

What this tells us is that there is some quantity, defined as A, which remains invariant regardless of the position of the beam. We will note that it can be shown that the value πA^2 corresponds to the area of the phase space ellipse, given by equation A.110. So we could define our emittance, ϵ as

$$\frac{\epsilon}{\pi} = \gamma(s)x(s)^2 + 2\alpha(s)x(s)x'(s) + \beta(s)x'(s)^2 \tag{A.111}$$

Where we divide by π since we are dealing with the area of an ellipse, defined as $A = \pi \cdot$ (length of major axis) $\cdot$ (length of minor axis).

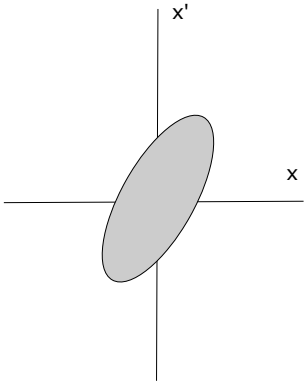

Figure A.4: An example phase space plot.

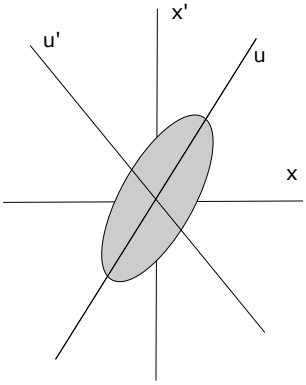

Figure A.5: Phase space plot with rotated coordinate system.

A.3.1 An alternative approach to calculating C-S parameters

The following method uses a statistical derivation of the beam emittance and Courant-Snyder parameters.

First, let us imagine a phase space plot for a beam. It might look something like Figure A.4. But calculating the area of this plot is rather difficult. It would be much easier if we were able to work in a coordinate system where the axes of the ellipse were aligned with the axes of the coordinate system. So we imagine for a moment that we can rotate our coordinate system about the origin until we create a new pair of coordinates, say u and u', which is illustrated in Figure A.5. What we now want to do is find a way to describe the emittance

in the new $u - u'$ coordinate system, using the $x - x'$ coordinate system. We can then find our variance in u and u' as below:

$$\sigma_u^2 =< u^2 >= \frac{1}{N}\sum_{i=1}^{N}(u_i - \bar{u})^2 \tag{A.112}$$

$$\sigma_u'^2 =< u'^2 >= \frac{1}{N}\sum_{i=1}^{N}(u_i' - \bar{u}')^2 \tag{A.113}$$

$$\tag{A.114}$$

Since we picked our origin at the center of mass of the phase space diagram, we have forced the conditions $\bar{u} = 0$ and $\bar{u}' = 0$. For this reason, those terms drop out and we're left with:

$$\sigma_u^2 =< u^2 >= \frac{1}{N}\sum_{i=1}^{N}(u_i)^2 \tag{A.115}$$

$$\sigma_{u'}^2 =< u'^2 >= \frac{1}{N}\sum_{i=1}^{N}(u_i')^2 \tag{A.116}$$

In our case, our axes are slanted such that σ_u is minimized and $\sigma_{u'}$ is maximized. This allows us to take advantage of the geometry of the ellipse when calculating our emittance. Since the emittance is defined as the area of the phase space, the area of our ellipse is simply

$$\epsilon = \pi\sqrt{\sigma_u^2\sigma_{u'}^2} \tag{A.117}$$

But our ultimate goal is to express this in terms of our x and x' coordinates. We can do this by assuming that our rotated coordinate system had a common origin and was changed by rotation through an angle θ. This allows us to turn our u and u' coordinates into x and x'

coordinates using our rotation matrix. Let us define the distance of the ith particle to the u' axis, in terms of the x and x' axes as

$$d_i' = |x_i' \cos(\theta) - x_i \sin(\theta)| = \sqrt{(x_i' \cos(\theta) - x_i \sin(\theta))^2} \tag{A.118}$$

We can get a similar equation for the distance between the ith particle and the u axis as

$$d_i = |x_i \cos(\theta) + x_i' \sin(\theta)| = \sqrt{(x_i \cos(\theta) + x_i' \sin(\theta))^2} \tag{A.119}$$

We start with the definition of the standard deviation of u' as

$$\sigma_{u'} = \frac{1}{N} \sum_{i=1}^{N} (d_i')^2 \tag{A.120}$$

$$= \frac{1}{N} \sum_{i=1}^{N} (x_i' \cos(\theta) - x_i \sin(\theta))^2 \tag{A.121}$$

$$= \frac{1}{N} \sum_{i=1}^{N} (x_i')^2 \cos^2(\theta) - 2\frac{1}{N} \sum_{i=1}^{N} x_i x_i' \sin(\theta)\cos(\theta) + \frac{1}{N} \sum_{i=1}^{N} (x_i)^2 \sin^2(\theta) \tag{A.122}$$

$$= < x_i'^2 > \cos^2(\theta) - 2 < x_i x_i' > \cos(\theta)\sin(\theta) + < x_i^2 > \sin^2(\theta) \tag{A.123}$$

$$= \frac{1}{2} \left(< x_i'^2 > (1 + \cos(2\theta)) - 2 < x_i x_i' > \sin(2\theta) + < x_i^2 > (1 - \cos(2\theta)) \right) \tag{A.124}$$

where we took advantage of trig identities for power reduction and double angles. Similarly, we can derive the result for the standard deviation of u as

$$\sigma_{u'} = \frac{1}{N} \sum_{i=1}^{N} (d_i')^2 \tag{A.125}$$

$$= \frac{1}{2} \left(< x_i'^2 > (1 - \cos(2\theta)) - 2 < x_i x_i' > \sin(2\theta) + < x_i^2 > (1 + \cos(2\theta)) \right) \tag{A.126}$$

Now, we know that our phase space shouldn't depend on the orientation of the ellipse, so it cannot have any dependence on θ at all, but only be a function of x and x'. Thus, we have the relationship

$$\frac{\partial(\sigma_{u'})^2}{\partial\theta} = 0 \tag{A.127}$$

Plugging in our result (equation A.124), and we have

$$\frac{\partial(\sigma_{u'})^2}{\partial\theta} = \frac{\partial}{\partial\theta}\frac{1}{2}\left(< x_i'^2 > (1+\cos(2\theta) - 2 < x_i x_i' > \sin(2\theta) + < x_i^2 > (1-\cos(\theta))\right) \tag{A.128}$$

$$= - < x_i'^2 > \sin(2\theta) - 2 < x_i x_i' > \cos(2\theta) + < x_i^2 > \sin(2\theta) \tag{A.129}$$

We can set this result equal to 0, and solve for our angle to get the relationship

$$\tan(2\theta) = \frac{2 < xx' >}{< x^2 > - < x'^2 >} \tag{A.130}$$

We're also able to use this equation to determine our values for $\sin(2\theta)$ and $\cos(2\theta)$ by trigonometry. This gives us

$$\sin(2\theta) = \frac{2 < xx' >}{\sqrt{(< x^2 > - < x'^2 >)^2 + (2 < xx' >)^2}} \tag{A.131}$$

$$\cos(2\theta) = \frac{< x^2 > - < x'^2 >}{\sqrt{(< x^2 > - < x'^2 >)^2 + (2 < xx' >)^2}} \tag{A.132}$$

We can substitute these results into A.124 and A.126 and get

$$\sigma_{u'}^2 = \frac{1}{2}\left(< x^2 > + < x'^2 > - \sqrt{(< x^2 > - < x'^2 >)^2 + (2 < xx' >)^2}\right) \tag{A.133}$$

$$\sigma_{u'}^2 = \frac{1}{2}\left(< x^2 > + < x'^2 > + \sqrt{(< x^2 > - < x'^2 >)^2 + (2 < xx' >)^2}\right) \tag{A.134}$$

Returning to our definition of emittance (equation A.117), we can now write

$$\epsilon = \pi\sqrt{\frac{1}{4}\left[(< x^2 > + < x'^2 >)^2 - (< x^2 > - < x'^2 >)^2 - (2 < xx' >)^2\right]} \tag{A.135}$$

$$= \pi\sqrt{< x^2 >< x'^2 > - < xx' >^2} \tag{A.136}$$

We can describe the area of the ellipse in the $u - u'$ coordinate system by the equation

$$\frac{u}{\sigma_u^2} + \frac{u'}{\sigma_{u'}^2} = 1 \tag{A.137}$$

Using our identities above and the ellipse from Hill's equation solution (A.110) we can give the following identities of our Courant-Snyder parameters in terms of the emittance and statistics of the beam thusly

$$\beta = \frac{\pi\sigma_x^2}{\epsilon} \tag{A.138}$$

$$\gamma = \frac{\pi\sigma_{x'}^2}{\epsilon} \tag{A.139}$$

$$\alpha = -\frac{\pi\sigma_x\sigma_{x'}}{\epsilon} \tag{A.140}$$